CORROSION RESISTANCE AND MECHANICAL PROPERTIES OF AMORPHOUS METAL HONEYCOMBS IN NaCl ENVIRONMENTS

By

CHANDRA SEKHAR MEDURI

Bachelor of Technology in Mechanical Engineering

Jawaharlal Nehru Technological University

Hyderabad, India

2012

Submitted to the Faculty of the
Graduate College of the
Oklahoma State University
in partial fulfillment of
the requirements for
the Degree of
MASTER OF SCIENCE
December, 2014

CORROSION RESISTANCE AND MECHANICAL PROPERTIES OF AMORPHOUS METAL HONEYCOMBS IN NaCl ENVIRONMENTS

Thesis Approved:

Dr. Jay C Hanan

Thesis Adviser

Dr. Kaan Kalkan

Dr. Raman P Singh

.

Acknowledgements

I would never have been able to complete this research work without the guidance of my thesis committee members, help from research-mates, and support from my family and friends.

First and foremost I would like to express my deepest gratitude to my advisor, Dr. JC Hanan, for all the advise, patience, guidance, and providing me an excellent atmosphere for doing research. It would be hard to overstate how much I benefited from his deep insight, perseverance and unwavering support. His scientist intuition and innovative ideas coupled with involvement in vigorous research will always be an inspiration to me. I would also like to thank him for giving me the opportunity and necessary financial support for my research. "I cannot wish for a better advisor than Dr. JC Hanan".

I would like to extend my gratitude to Dr. K Kalkan, for always willing to help and give his best suggestions. I would also like to thank Dr. Ravi Vilupanuri and his team for their help and guidance in successfully completing corrosion testing. I gratefully thank Dr. Kaan Kalkan and Dr. Raman Singh for being in my thesis committee amidst their busy schedule. I would like to extend my thankfulness to Dr. M Allakharami, Balaji Jayakumar, Sudheer Bandla, and Vahid for their continuous support from the past two years.

It is my pleasure to express my wholehearted gratitude to my friends Chaitanya, Sravya, Harsha, Nitesh, Divya, Venkat, Kunal, Nikhil, Ozge, Aditya, and Lukasz.

Finally, I would love to express my appreciation to my parents, who are always there motivating and cheering me up.

Acknowledgements reflect the views of the author and are not endorsed by committee members or Oklahoma State University.

TABLE OF CONTENTS

Chapter Page

LIST OF TABLES

Table Page

LIST OF FIGURES

Figure Page

CHAPTER I

INTRODUCTION

Honeycombs are anisotropic light weight cellular structures that are commonly used as cores in sandwich panels. In a typical sandwich composite, the core carries normal and shear loads in the out-of-plane direction. Honeycombs have high stiffness and strength-to-weight ratio in the direction perpendicular to the axis of the honeycomb cells, with applications ranging from packaging to aircraft panels, navel runway bases and space structures. The out-of-plane properties, mainly, axial compressive strength of the honeycomb is critical in a sandwich composite construction. Mechanical properties of honeycombs depend on base material properties (such as yield strength $\{\sigma_y\}$, Young's modulus $\{E_s\}$) and geometry of the cell. Geometry of the cell includes the thickness of the cell wall (also known as foil gauge) and cell size (Figure 1). The ratio of cell wall thickness-to-cell size, designated by "*t/l"* is a critical geometric parameter. Therefore a change in thickness of the cell wall influences the overall mechanical behavior of the honeycomb and the composite.

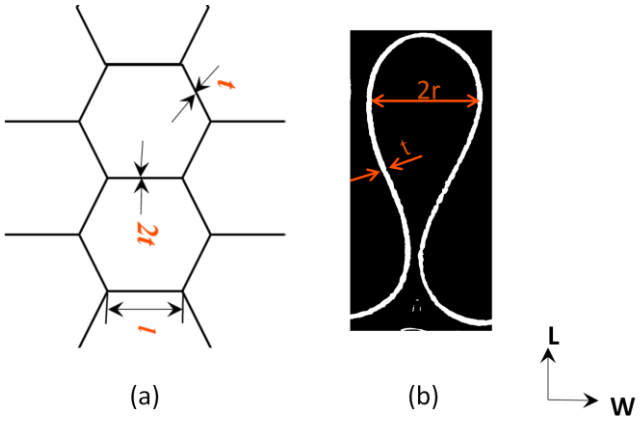

Figure 1 Different geometric parameters of (a) Aluminum Honeycomb (Al-H) unit cell (b) Amorphous Metal Honeycomb (AMH) unit cell.

Sandwich structures used in applications such as aerospace structures can be subjected to numerous degrading phenomena that will affect the mechanical properties and threaten the integrity, safety, and service life. Degradation mechanisms include creep, debonding of face sheets, stress cycles (fatigue), and corrosion [1]. Corrosion is one of the most critical reasons for strength degradation. It is an unavoidable phenomenon for most metals, especially in harsh environments. For example, an aircraft component can be subjected to different types of environments, namely, hot/cold weather conditions [2], desert conditions, and seawater conditions. Metallic structures when exposed to such environments corrode. In the case of honeycombs used in aircraft, corrosion happens mainly because of moisture ingression into the cells of the honeycomb [3]. Moisture ingression will result in corrosion of the base material, debonding of adhesive joints, and fracture of cell walls [4]. Corrosion of the base material not only causes loss of material but also results in degradation of strength and core-face debonding. This will greatly affect the integrity of the structure as a whole. Aluminum honeycombs are the most widely used metallic honeycombs in aerospace applications [14]. They are susceptible to corrosion in chloride containing environments and results in localized or pit corrosion [5, 7]. Steels, paper, polypropylene, and meta-aramid material (commercially

known as Nomex) have also been used as honeycomb base materials in various applications. Replacing aluminum with more corrosion resistant materials such as stainless steel or titanium often compromises specific strength (strength –to-weight ratio), which is a main design parameter in aircraft components. So improving the corrosion resistance of aluminum was a better alternative. Corrosion resistant coatings have been used. These coatings do not help in increasing the strength but add weight. This results in a reduced honeycomb strength-to-weight ratio. If possible, the selection of a honeycomb base material with good mechanical properties and corrosion resistance is a better alternative.

Corrosion is an electrochemical reaction involving two chemical processes, oxidation and reduction [6]. Corrosion of a metal can occur only when there is a

1. Positive or anodic area, "Anode"
2. Negative or cathodic area, "Cathode"
3. Path for flow of ionic current, "Electrolyte"

When a metal is exposed to harsh environments, both anodic and cathodic regions are observed on the same metal surface. Here the environment acts as an ionic carrier and bulk of the metal acts as an electron carrier from anode to cathode. The high energy regions on the surface of a metal will act as anodic regions and less energetic regions act as cathodic regions [6, 7]. Generally in a crystalline material, grain boundaries and mechanically stressed regions will be relatively high energetic regions. This makes grain boundaries and crystal defects acts as active sites for corrosion in crystalline materials [6].

Metallic glasses are non-crystalline materials with no crystal defects such as grain boundaries and dislocations. Chemical homogeneity, disorder, and free volume characterize the atomic structure of an amorphous metal. They have exceptional mechanical and chemical properties. They have high elastic strain (up to 2% when compared to 0.2% of crystalline materials [9]), high Young's modulus

(up to 195 GPa [8]), and high strength (up to 5 GPa [10]). The absence of defects such as grain boundaries make them potentially more corrosion resistant compared to their crystalline counterparts. High yield strengths, Young's modulus and corrosion resistance makes them also favorable for use as honeycomb base materials. Recently, amorphous metal honeycombs with unprecedented specific strength have been demonstrated [11]. Metallic glass ribbons manufactured using rapid solidification techniques at a cooling rate of 10^4-10^6 have been processed into "teardrop" shape to form a honeycomb. Individual cells formed are held together using adhesives. Though the adhesives currently used in making amorphous metal honeycombs are giving good compressive strengths, they lack the ability to retain their holding capacity when exposed to humid environments.

At lower cell size [11] shear bands are formed in the cell walls of honeycomb. These amorphous metal honeycombs, with the advantage of an amorphous metal base material, are expected to be more corrosion resistant than crystalline aluminum honeycombs. Estimating the effect of corrosion on the mechanical properties of the Amorphous Metal Honeycombs (AMH) is important in this regard.

In this thesis, Corrosion behavior of AMH is studied in accelerated NaCl environments. Mass and thickness losses were measured to evaluate corrosion resistance and the effect of corrosion on mechanical properties. Mass loss measured using analytical balance was used to calculate the corrosion rate while thickness loss measured using radiography was used in evaluating the compressive strength of AMH.

CHAPTER II

LITERATURE REVIEW

2.1 Corrosion of honeycombs: Moisture ingression

Moisture ingression is an unresolved issue in the aircraft industry, and is more predominant in honeycombs. "The case against Honeycomb Core [4]"attributes the negative effects of moisture ingression such as weight gain and strength loss to the intrinsic property of honeycomb. It is known that moisture ingression in honeycomb core sandwich structures always occurs on some level and causes damage in industry products such as aircraft etc. (Cise and Lakes 1997). The moisture ingression rate depends on direction and position of the core, core structure, and material properties of the core and face (Shafizadeh et al 1999). Fogarty (2009) summarized that the proper design of honeycomb core structures and the choice of face and core materials can reduce or even prevent moisture ingression. However, for the sandwich panels containing Kraft paper honeycomb cores and wood composite skins, the moisture does not only affect the core structure, but also the material properties of core paper and wood skin**.**

In an aircraft, outboard flap wedge, upper fixed wing panels, nose landing gear door, escape slide door and the main landing gear door are more susceptible to moisture ingression as compared to

other components [13]. Sources of moisture ingression include but are not limited to closeouts, manufacturing imperfections, attachments, thin aerodynamic face sheets, and foreign object damage, which are inevitable features of real world processes [12]. It can also be due to poor sealing during repairs and at panel edges. The two important modes of moisture ingression are a) Direct ingress and b) Indirect or Diffusion ingress.

In simulated environments, though quantitatively both the strength losses are similar, diffusion ingression results in recoverable strength loss whereas direct ingression results in non-recoverable strength loss after drying [14]. Direct ingression through face sheet is more detrimental as the presence of water in the honeycomb will destroy the honeycomb through a "*freeze-thaw mechanism"* [15]. Damage of the face sheet not only results in moisture ingression but also exposes honeycomb to harsh environments. At different operating conditions, the temperature inside the honeycomb core varies from -40^0C to 100^0C [16]. At lower temperatures, water in the honeycomb core will freeze. As the freezing water expands, it stresses the honeycomb cell walls. At moderate temperatures, frozen water melts and honeycomb walls relax. After a number of these cycles, cell walls will catastrophically fail. Whereas at elevated temperatures, water vaporizes and the pressure inside the cell walls can exceed the tensile strength of the adhesive bond between core and face sheet. This will lead to delamination of the face sheet [17].

Moisture ingression also results in corrosion of the honeycomb base material. Harmful and irreversible effects of direct ingression on strength loss are associated with surface corrosion of honeycomb, not the composite or adhesive components of the sandwich [12]. "Adhesive degradation" i.e. bond failures associated with separation of the core from face sheets or failure of node bonds in the honeycomb is an important issue. Base material corrosion is however more detrimental [13, 17]. An evaluation of performance of sandwich structures for F-111 exposed to moisture for moisture for 6 months shown 50% reduction in Flatwise-Tensile Strength and 63% reduction in shear strength. Observed reduction was due to corrosion of the aluminum core [17].

Aluminum has an inherent defense mechanism to counter corrosion. It forms stable corrosion inhibiting oxide layer (patina). Even though the passive oxide layer is resistant to atmospheric gases, soil and moisture, it is susceptible to damage in the presence of hydrochloric acid, wood preservatives, lead-based paints, and chloride containing environments (such as seawater environments). Replacing aluminum with more corrosion resistant materials such as stainless steel or, titanium compromises the specific strength (strength –to-weight ratio) and specific cost that are main design parameters in aircraft components.

Perforated honeycombs were also used in some space applications [18] and these holes served as a path for moisture resulting in corrosion. The resulting moisture ingression (direct ingression) was more detrimental because of direct exposure of metallic surfaces to water (electrolyte). This necessitated the use of corrosion resistant coatings to avoid corrosion damage. Corrosion resistant coatings comprise of a base layer underlying a primer layer. Coatings such as CR-III, CR-PAA have been used as base layers for improving the corrosion performance of aluminum honeycombs. CR-III consists of an organo-metallic polymer and chromate-based protective layer whereas CR-PAA is phosphoric acid anodized coating. CR-PAA, apart from improving the corrosion resistance, provides superior performance with regard to adhesive bond strengths, hot/wet and salt spray environments, and crack propagation. These coatings necessitated the use of primers for a strong adherend-adhesive bond (Figure 2). Use of these coatings resulted in an increase of non-structural mass. This in turn reduced the strength-to-weight ratio of the honeycomb as a whole. This necessitated a shift towards high performance materials, which inherently have excellent corrosion resistance and high specific strength. Amorphous metals are one potential option.

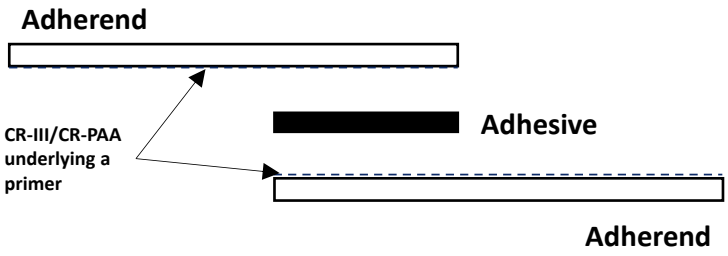

Figure 2 Adhesive joint of a corrosion resistant coated honeycomb.

2.2 Metallic Glasses:

Amorphous, or glassy metal systems have been extensively studied since their introduction in 1960s [19] because of their structural, mechanical, magnetic, electronic, and corrosion properties [9]. Some important properties, both attractive and unattractive, are shown in Table 1. There has been an increasing interest in the corrosion behavior of bulk metallic glasses (BMGs) [20]. Corrosion resistance is a critical factor for the consideration of their use in chemical or harsh environments. Corrosion properties of an amorphous alloy are expected to be superior to its crystalline counterparts due to their lack of local microstructure features and chemical homogeneity. This section focuses on providing an overview of corrosion resistance of amorphous metals (factors effecting corrosion resistance, and corrosion mechanisms) in general and Fe-based amorphous metals in particular.

Table 1 Pros and Cons of metallic glasses

Attributes	*Pros*	*Cons*
General	• Absence of grain and phase boundaries • No compositional variation [9] • Near-atomic scale features [19]	• Present processing and component cost [21] • Compositional optimization for glass-forming ability hinders optimization for other properties [9]
Mechanical	• High hardness, giving good wear and abrasion resistance [19] • High yield strength [9] • High specific strengths • High resilience per unit volume	• Zero ductility in tension because of severe localization of plastic flow (shear bands) [21] • Fracture toughness and toughness can be variable [9] • Larger components may fail in brittle manner due to small process-zone size • Embrittled by annealing [22]
Chemical	• Lack of grain boundaries, and associated microstructural features (like solute segregates) gives good corrosion resistance [9, 21,22,23] • Sensitive to compositional changes [22, 24, 25, 26, 27]	

An amorphous metal, by definition has a disordered atomic arrangement resembling a liquid and has no long-range order. Recently, medium-range order in amorphous metals has been identified [23]. The main features of these materials that resulted in their superiority are: atomic structure, the absence of grain boundaries (crystal defects) and a wide range of alloy compositions over which single-phase metallic glasses can be formed [21]. Several metallic glass alloys that have been

studied for their corrosion performance include Zr-based [22], Ni-based [34], Cu-based [25], Fe-based [24, 26, 35, 36], Mg-based [37], and Al-based systems. Most of these studies are comparison of crystalline and amorphous alloys of same composition. For efficient utilization of these amorphous metals comprehensive information over a range of corrosion modes like general corrosion, galvanic corrosion, and localized corrosion; including corrosion fatigue, stress corrosion cracking, and hydrogen damage is needed. Limited information is available on corrosion modes of some alloy systems and there is no established theory that can explain corrosion mechanisms across different alloy systems [20]. Though there are some studies on general and localized corrosion mechanisms in BMGs [38], the majority of the electrochemical studies prioritize the corrosion resistance of new compositions. The quest for BMG alloys with increased glass-forming ability resulted in an influx of new compositions and study of their corrosion resistance is important for their applications.

For the same alloy composition amorphous metals are more corrosion resistant than their crystalline counterparts. However, this is dependent on the type of electrolyte that they are exposed to [22, 25]. For example, the corrosion resistance of amorphous ($Cu_{50}Zn_{50}$) is marginally more than its crystalline form in 1N NaCl electrolyte but is almost the same in $NaClO_4$ electrolyte

2.2.1 Corrosion Resistance of Metallic Glasses:

Corrosion resistance of metallic glasses can be attributed to several factors, - some of which are listed below:

- The capability to form a single phase solid solution with good chemical and structural homogeneity, this eliminates associated microstructural defects and second phase particles.

- The addition of rare earth, transition, and refractory elements result in improved passivity [24]. So the ability to form solid solutions with these additives is important for corrosion resistance as it results in passivity of these metals.
- The addition of metalloids (minor alloying elements) does not improve corrosion resistance; rather they are important in enabling amorphous structure at low cooling rates.
- Effectiveness in repassivation of local corrosion resistance once the passive film is dissolved.

2.2.2 Importance of Amorphous Structure:

Amorphous alloys are typically manufactured using the following processes:

- Rapid quenching (melt spinning)
- Solid-state reaction (with or without diffusion)
- Mechanical treating (mechanical alloying)

The rapid cooling rates involved in production of these amorphous alloys inhibit solid-state diffusion and promote chemical homogeneity. The short time available for diffusion suggests that these alloys lack second phases, segregates and precipitates. Though there are studies [28, 29, 30, 31] showing the presence of second phases in some BMGs, the observed crystalline inclusions (second phases) are a result of heterogeneous nucleation caused by impurities in the melt [29, 32, 33]. From an electrochemical aspect, chemical homogeneity and lack of segregates or second phases are advantageous as they result in corrosion by forming micro-galvanic cells.

Not all the metallic glasses, even in their fully amorphous form, are corrosion resistant. Major constituents, like Fe, Ni, Zr, Mg, Cr etc. are inherently active when exposed to aqueous environments and readily react with oxygen to form corrosion products. Nature of these oxide layers (patinas), which includes ability to hinder electrolyte from contacting metal surface and durability of

passive layer formed, determines corrosion resistance of the alloy. Therefore, corrosion properties are related to amorphous structure and chemical composition of the alloy. Thus chemical and structural homogeneity, possibility of forming wide range of chemical compositions, and amorphous structure are important factors to be considered for evaluating corrosion resistance of metallic glasses.

Comparative studies between crystalline and amorphous forms of alloys $Zr_{41.2}Ti_{13.8}Cu_{12.5}Ni_{10}Be_{22.5}$ [22], $Cu_{50}Ti_{50}$ [25], and $Cu_{50}Zn_{50}$ [25] substantially explained the effect of microstructure on the material properties in general and electrochemical corrosion in particular.

2.2.3 Importance of Alloy Composition:

Passive layer is usually an oxide film of an element in the alloy. Most of the simple Fe-, Cu-, and Ni-metalloid glasses passivate in alkali just like crystalline alloys. This passivation ability was found to be poorer when compared to crystalline metals in acidic or neutral media in case of $Cu_{50}Ti_{50}$, $Cu_{50}Zn_{50,}$ and Fe-C-Cr-Mo alloys [25, 39]. To overcome this, replacement of Fe with more noble metals (Cu, Pd, Rh) or more readily passivated metals (Cr, Mo, Zr, Ti, W) have been done [39, 40]. Chromium in particular was the most effective. In this aspect, metallic glasses resemble stainless steels but the amount of chromium required for good passivation is lesser for metallic glasses. Fe-based amorphous alloys containing 8% Cr showed a similar corrosion resistance as Fe-based crystalline alloys containing18% Cr [20]

This implies that formation of a passive layer depends on the alloy composition. A metallic glass can typically have metals and metalloids. The role of these has to be dealt with separately in order to assess their relative roles in passive film formation.

The Influence of Metal:

The main alloying metals in Fe-based metallic glasses are Mo, Mn, Ti, W, Cr, Ni, Zr, and Fe. These metals contribute to the passive oxide layer formation. Every element has a special role in the passivation of a glass. For example, Cr forms oxyhydroxide $CrO_x\ (OH)_{3-2x}.\ nH_2O$, a key compound in passive films of Cr-containing alloys. Ti also forms a protective layer, but Cr has been more effective in improving corrosion resistance [35]. Metals like Mo, and W are also effective in promoting anodic passivation. However, their presence inside passive film has not been detected [39]. Their role in passive film formation is crucial in certain alloy systems, such as Mo in the (Fe, Cr) alloy system [35, 36]. The passivating capability of glasses containing unique combination of Cr, Mo, and P (metalloid) was remarkable, as it passivated even in 12M HCl [40]. Similar improvement in the corrosion resistance of Fe-xNi-13P-7C with the addition of Ni in neutral chloride electrolyte has been observed [41]. The rise in the corrosion potential of amorphous Fe-Ni alloys is due to the reduction of the anodic reaction.

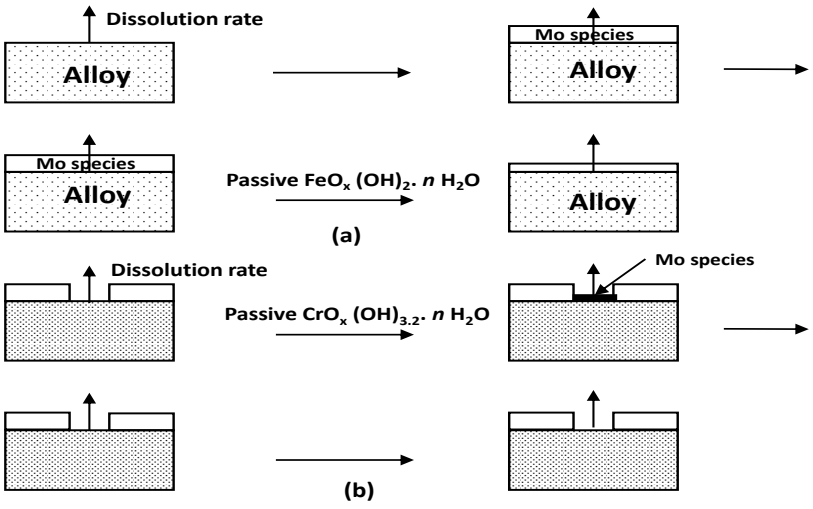

Figure 3 Diagram to show importance of Mo in Fe-based amorphous alloy during (a) Passivation (b) Repassivation in acidic media (also has Cr) [35]

The Influence of Metalloid:

Similar to alloying metals, the role played by metalloids has been addressed by several authors [35, 38]. Metalloids help in formation of the amorphous structure during rapid quenching from melts

Metalloids, if present in large amounts accelerate active dissolution of the alloying elements. This results in rapid formation of a passive film [42]. Metalloids also help in enriching the passive film with oxide forming metals, such as phosphorous in the Fe-Cr system. Though chromium has been effective in improving corrosion resistance of Fe-based alloy systems, a study [41] found that the addition of Cr to Fe-B-C and Fe-B-Si amorphous alloy systems was not effective in improving corrosion resistance. This shows the effect of an individual metalloid on the corrosion resistance of these glassy alloys.

P in Fe-Cr alloy system is a good example [41, 42]. As shown in fig, amorphous Fe-Cr-13P-7C alloy containing more than 8% Cr showed spontaneous passivity and no weight loss in several neutral and acidic media. This high corrosion resistance was interpreted in terms of uniform passive film enriched with Cr [43], and rapid re-formation of the film. Uniformity of passive film is related to chemical homogeneity of the alloy, which has no dependence on the change in metalloid additive [43]. For the formation of a passive film, it was found that the presence of P enhances the active dissolution of alloys and results in rapid enrichment of Cr in the alloy-solution interface. The rise in corrosion potential of this alloy is due to suppression of the anodic potential rather than raising the cathodic potential.

2.2.4 Corrosion Mechanisms in Metallic Glasses

Corrosion mechanism of amorphous alloys is similar to conventional crystalline materials. It involves oxidation and reduction reactions. Oxidation on the material surface produces loss of material in form of loss of electrons and ions. Electrons lost are used to calculate corrosion rate by

Faraday's Law in electrochemical studies. Similarly the loss of ions (mass) is used to calculate corrosion rate in gravimetric methods. If the alloy exhibits an active-passive nature in the environment, then dissolution of metal ions will result in the formation of a passive film. A nonporous, continuous and adhering (to metal surface) film will decrease the corrosion rate. This is because the mechanism of migration of ions through the passive film is slow solid-state diffusion. Also a film that is a poor conductor of electrons will further decrease the corrosion rate.

BMGs are generally homogeneous materials. Accordingly, their susceptibility to pitting corrosion should be less than in crystalline alloys. However, the presence of physical or chemical inhomogeneities in BMGs resulted in their susceptibility to pitting [38, 44]. Gebert et al. [44] reported a chloride attack at the transition zone between the amorphous matrix and crystalline inclusion of Zr-based BMG. This transition zone was compared to a grain boundary in a crystalline material. An adsorption mechanism was suggested to explain observed pitting. According to this, chloride ions are preferentially adsorbed at weak portions of the passive film. These weak portions are active regions of passive film that are located over the transition zones. This results in localized attack or pitting [44, 45]. The migration of chloride ions to the active regions leads to local selective dissolution of elements. This localization can also be due to changes associated with chemical composition of these transition zones or overlying passive film. In all, chemical factors dominate the susceptibility of amorphous metals to pitting corrosion. That is, some elements due to their nature are more resistant to localized corrosion. Thus, the localized corrosion resistance of amorphous alloys is predominantly dependent on alloy chemistry. This is because chemical homogeneities affect the protectiveness of the passive film more so than physical defects [38]

Also lack of grain boundaries retards ionic movement, which otherwise can result in reactions leading to corrosion. Not all the amorphous oxides will result in improved corrosion resistance. Desirable properties include bond flexibility, defect free and ductile film, efficient and rapid repassivation.

Though the ability to form an amorphous oxide layer that acts as passive film depends mostly on the alloy composition, the advantage of having a homogeneous single phase alloy underneath the passive layer hinders the nucleation of corrosion. The amorphous structure as a whole is not without defects, but not having major defects such as grain boundaries in crystalline metals adds to the durability of the passive film.

2.3 Aluminum and Amorphous Metal Honeycombs

High specific strength (strength-to-weight ratio) and, corrosion resistance, are the most desirable properties for an aircraft structural component [7]. For this reason, aluminum alloys, steels, with corrosion resistant coatings, became commonly used materials. Depending on deformation mechanism and manufacturability different base material honeycombs have different cell shapes. For example, aluminum honeycombs are manufactured in hexagonal and corrugated shapes. The plasticity of the aluminum helps in attaining a hexagonal cell shape. Since the application of this expansion method is limited to materials that can deform plastically. Recent efforts have shown the possibility of high strength Fe-, Zr-, Pt- based BMG honeycombs [11]. Metallic glasses (MGs) show very little or no plasticity. In MGs, plastic deformation takes place through the on-set of shear bands. These shear bands are considered defects. The formation of a hexagonal cell shape involves 6 to 8 plastic hinges. This means that if we form a hexagonal MG cell then shear bands will be formed in all 6 plastic hinges. These act as defects and weaken the honeycomb. Also the high elastic strain (2% compared to 0.2% in crystalline materials) limits the use of expansion method to form metallic glass honeycombs.

Recently, a novel bottom-up approach was developed to manufacture Amorphous Metal Honeycombs (AMH). In this manufacturing approach, amorphous $Fe_{45}Ni_{45}Mo_7B_3$ (MB2826) ribbons are manufactured in to a cellular network of a “teardrop” shape. Thin MB2826 ribbons are folded in to a teardrop shape and bonded using an adhesive. Honeycomb as dense as 0.6 Mg/m^3 and

cross-section of 12 in x 12 in were manufactured [11]. Theoretically high compressive strengths can be achieved with these AMH. AMH gives better specific strengths than Al-H after a certain density. Specific strengths as high as 150 KNm/Kg were achieved with AMH. Other techniques such as *pin method* and, *comb method* are also used in the formation of teardrop. The high cooling rates involved in the manufacturing of MGs is thought to induce thermal residual stresses.

Table 2 Out-of-plane properties of aluminum and amorphous metal honeycombs

Property	**Aluminum Honeycomb**	**Amorphous Metal Honeycomb**
Density $\left(\frac{\rho^*}{\rho_S}\right)$	$1.54\left(\frac{t}{l}\right)$	$2.06\left(\frac{t}{r}\right)$
Compressive strength	$7.14\sigma_y\left(\frac{\rho^*}{\rho_S}\right)^3$	$2.63E_s\left(\frac{\rho^*}{\rho_S}\right)^3$
L direction Shear strength	$1.51\mathrm{E_S}\left(\frac{\rho^*}{\rho_S}\right)^3$	$1.26\mathrm{E_S}\left(\frac{\rho^*}{\rho_S}\right)^3$
W direction Shear strength	$0.98\mathrm{E_S}\left(\frac{\rho^*}{\rho_S}\right)^3$	$0.31\mathrm{E_S}\left(\frac{\rho^*}{\rho_S}\right)^3$

From Table 2 it can be seen that the mechanical properties of these honeycombs depend on the following:

1. Linearly with the Young's modulus or yield strength of the material
2. Cubically with the thickness of the cell wall

Corrosion of a metal will result in loss of material. When applied to honeycombs, corrosion of the base material will result in loss of thickness of the cell wall, which has a cubical effect on mechanical properties of honeycombs. So a study of base material corrosion properties will help in

estimating the effect of corrosion on mechanical properties of the honeycomb. Corrosion monitoring is defined as the practice of acquiring information on the following

- Corrosivity of the environment surrounding the material
- Progress of corrosion-induced damage to the material

2.4 Corrosion Monitoring Techniques:

Corrosion monitoring provides performance data, a basis for life prediction, and is one of the important components in corrosion prevention and control. A wide variety of corrosion measurement techniques are used for corrosion monitoring. They are

i. Gravimetric Techniques: Weight loss analysis.
ii. Electrochemical Techniques: Linear polarization, potentiostatic and potentiodynamic measurements, electrochemical noise methods, galvanic sensors.
iii. Non Destructive Testing Techniques: Ultrasonic testing, Radiography, Thermography, Eddy current/magnetic flux.
iv. Others: Electrical resistance techniques, hydrogen permeation methods, radioactive methods.

Among these Weight loss analysis and Radiography have been used in evaluating corrosion behavior of Fe-based metallic glasses.

2.4.1 Weight loss:

Weight loss analysis is the simplest and long-established method of estimating corrosion losses. A weighed metal sample is introduced in to the desired environment, and later removed after a reasonable time interval. The removed sample is then cleaned and reweighed. The resulting weight loss, exposed area, and time of exposure are used to calculate corrosion rate (CR). This technique is useful in visual inspection, observing and analyzing corrosion deposits.

2.4.2 Non-Destructive Testing (NDT):

NDT procedures have been used to a good extent in corrosion evaluations. Use of these procedures, especially radiography, has shown to give considerable advantages such as cost and time savings, evaluations of complex and inaccessible parts, indicate nature and degree of attack, insulation and coatings need not be removed. Radiographic (X-ray) techniques have been used to measure thickness or change in thickness quantitatively. Recently it has been shown that digital radiography, automated radiography, and tomography are used for in-service evaluation of pipes [46, 47, 48]. In this regard, different techniques, namely, tangential radiographic projection technique (TRT), double wall inspection technique (DWT) have been formulated based on the samples to be evaluated [49].

2.5 Accelerated Corrosion Testing: 3.5% NaCl immersion and Salt Spray

Immersion testing is one of the most widely used laboratory techniques for evaluating corrosion resistance, by simulating real world environments in the laboratory. The simplest, long-established method of estimating corrosion loss is weight loss analysis. A known weight sample (coupon) of the metal under consideration is introduced into the process. After a reasonable time interval the coupon is removed, cleaned of all corrosion products and reweighed. The weight loss is converted to corrosion rate or metal loss. Corrosion rate is the usual measure of corrosion loss in these tests. When accelerated testing is needed, electrochemical (ex: polarization techniques) and salt spray or salt fog (ASTM B117) testing are employed. Corrosion rate is a measure of the rate of corrosive attack. The rate of corrosive attack depends on corrosion resistance of the material and corrosivity of the environment. The interrelation was explained using [50]

$$\text{Rate of corrosive attack} = \frac{\text{corrosivity of environment}}{\text{corosion resistance of material}} \qquad \text{Equation I}$$

From the above relation, it can be interpreted that

- For a given material, rate of corrosion increases with an increase in corrosivity of the environment.

- For the given corrosivity of the environment, rate of corrosion is inversely proportional to corrosion resistance of material.

For a given material, all these testing techniques are largely dependent on corrosivity of the environment i.e. electrolyte. While the selection of testing technique depends on the time frame in which testing needs to be completed, selection of the electrolyte depends on the environment that needs to be simulated. The main aim of these accelerated tests is to develop reliable data in a much shorter time frame than in natural environments. A number of studies have been conducted on the use of synthetic environments that will yield results comparable to those in natural environments. In many cases, both accelerated tests and simulated environments were successful in predicting the relative corrosion behavior of materials. But the corrosion data produced in such simulated environments is reliable second only to in-service conditions.

2.5.1 3.5% NaCl:

Even though the corrosion behavior of different types of materials can be assessed either in natural and synthetic environments, each have their own advantages and disadvantages. For example consider the design of a synthetic test to simulate the corrosion behavior of a material in seawater environment. Variation in world's seas with respect to pH, salinity, dissolved salts, temperature, oxygen, biological influences; will affect the material performance. The most common electrolytes used in simulating seawaters are synthetic seawater (ASTM D1141) and 3.5% NaCl. All the major inorganic components of seawater can be reproduced by synthetic seawater, but the results from these are significantly different from natural seawater. The main reasons behind these differences can be attributed to the nature of complexes or ligands that can be formed with metallic ions, biological organisms and the buffering capacity of natural seawater. From a material point of view,

the corrosivity or severity of a testing solution varies from material to material. For example, sprays of natural seawater (NSW) resulted in a weight loss much lower than sprays of 20% and 3% NaCl in case of Zn, while sprays of NSW is more severe than 20% NaCl in case of ingot iron containing 0.04% Cu [51]. Although, simulated seawaters do not give accurate results, they are used for estimating the effect of natural seawater. This is because the conductivity of these simulated seawaters is in agreement with the natural seawater.

Table 3 Comparison of conductivities of Natural and Synthetic (ASTM D1141, 3.5% NaCl) Seawaters [51]

	Natural Seawater	**ASTMD1141 Seawater**	**3.5% NaCl**
Conductivity (mS/cm)	53.2	52.7	55.4

In case of NaCl Immersion tests, maximum corrosion rate occurs close to 3.5% NaCl concentration as shown. This is the approximate salt content in full-strength seawater. This makes seawater a good corrosive environment.

The pH of 3.5 % NaCl solution is around 8-9. In the pH range of 4-10, the rate of corrosion is independent of pH (Figure 5) and depends mainly on the diffusion of oxygen to the metal surface. In this regime, corrosion can be varied by the amount of dissolved oxygen. The corrosion rate can be accelerated by maintaining a concentration of 12 ml/lit dissolved oxygen. In general oxygen can be added by dissolving hydrogen peroxide (H_2O_2) or connecting to an external oxygen source.

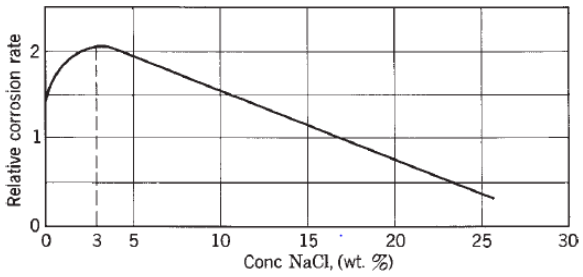

Figure 4 Effect of corrosion rate of Iron in aerated solution at room temperature on NaCl concentration [52].

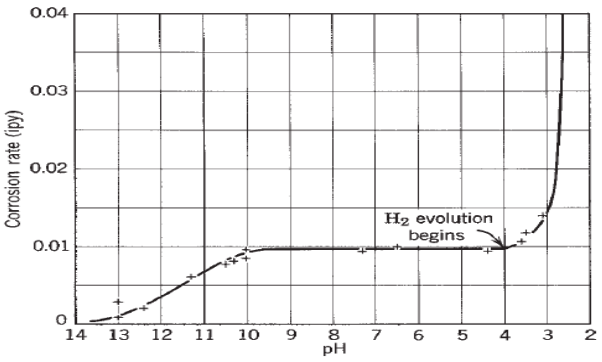

Figure 5 Effect of pH on corrosion rate dependence of iron in aerated soft water [53].

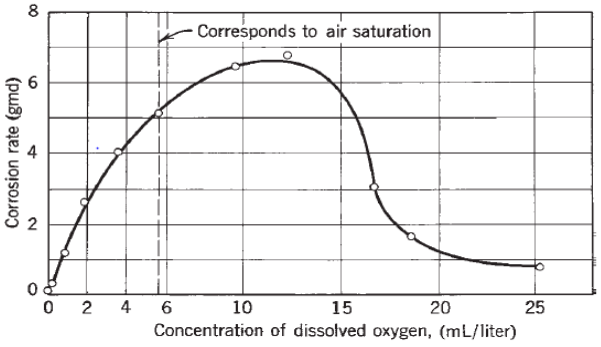

Figure 6 Effect of concentration of dissolved oxygen on corrosion rate of mild steel in slowly moving distilled water at room temperature [53].

2.5.2 Salt Spray:

The purpose of an accelerated corrosion test is to duplicate, in the laboratory, the performance of a product in the field. The salt spray test has been used extensively for this purpose. It has been extensively used for comparison purposes. An extensive amount of literature is available on study of ranking different materials using salt spray tests.

CHAPTER III

MATERIALS AND METHODS

3.1 Parent Material - Metallic Glass Ribbon (AMR)

One amorphous metal under investigation is an Fe-Ni based amorphous alloy. In addition to Iron and Nickel, it has smaller amounts of Molybdenum, Boron, and trace amounts of Cobalt, Carbon, and Phosphorous. The chemical formula is $Fe_{45}Ni_{45}Mo_7B_3$. Commercially these are manufactured by Metglas Inc. in the form of ribbons as shown in Figure 7

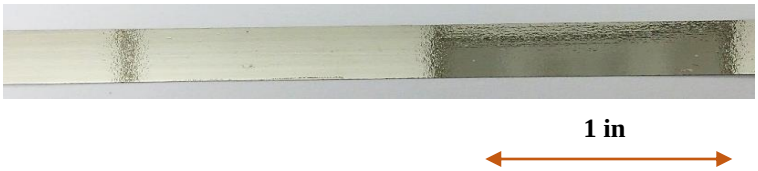

Figure 7 As-received Fe-Ni based Metallic Glass Ribbon (AMR).

3.1.1 Physical Properties of $Fe_{45}Ni_{45}Mo_7B_3$ ribbon:

These metallic ribbons are available in the form of rolls, widths in range of 2.5 mm to 25 mm and thickness of 29 microns. A width of 8 mm was chosen in this testing. They have a distinguishing shiny and mathe surfaces. The rated density of these ribbons is 7.9 Mg/m^3. They are used in transformer cores because of their magnetic properties. Besides good magnetic properties such as DC permeability, saturation magnetostriction, and electrical resistivity; $Fe_{45}Ni_{45}Mo_7B_3$ has tensile strength of 1-2 GPa, Elastic Modulus of 100-110 GPa.

In order to study their mechanical properties, these ribbons were subjected to tensile loading. ASTM E345-93, "Standard Test Methods of Tension Testing of Metallic Foil and ASTM E8, "Tension Testing of Metallic Materials" was followed for sample preparation and tension testing respectively.

Tension testing of thin ribbons can be a challenge. In order to facilitate proper gripping of the ribbons, aluminum tabs were glued to both ends of the ribbon using epoxy as seen in Figure 8. Then tension testing was carried out on a screw driven Instron 5572 materials tester. Over a gauge length of 50 mm, a strain rate of 0.2mm/min was applied.

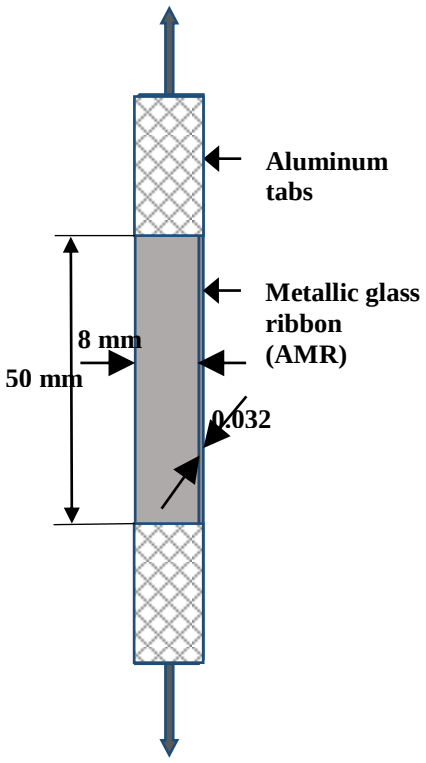

Figure 8 Sample preparation for tension testing of AMR.

3.1.2 AMR with shear bands:

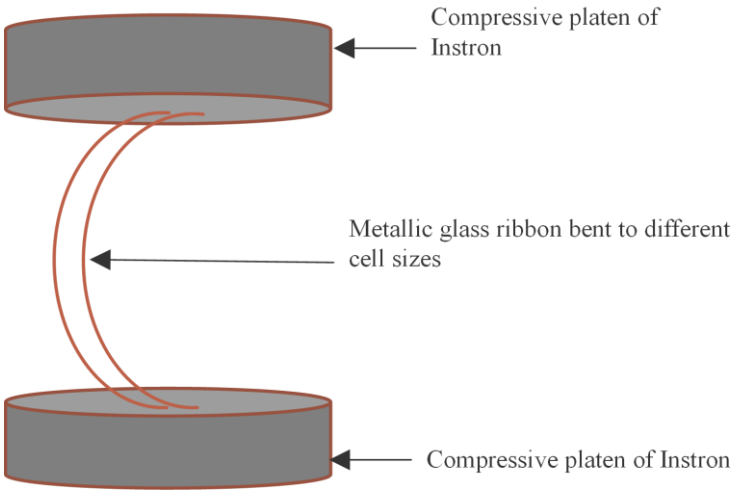

Figure 9 Set up for AMR bending test.

AMH of different cell sizes can be manufactured using the methods described here. Shear bands, a form of plastic deformation in metallic glasses, is not seen in all cell sizes. Propagation of shear bands is prominent at lower cell sizes. They may change the mechanical or corrosion behavior of the resulting honeycomb, so identification of a critical cell size below which shear bands can be observed is useful. A "ribbon bending test" (Figure 9) was performed to calculate the critical cell size. In this test the ribbon was attached to the two compressive platens of an Instron 5572 material tester. Here the distance between the two platens gave the cell sizes while the force required to bend the ribbon was used to estimate the force required to hold the cell in position.

Using a bottom-up approach of making an AMH, shear bands can be formed in the AMR. Here this was done by bending the ribbon around a pin of 1.2 mm diameter. These pins along with a pin holding

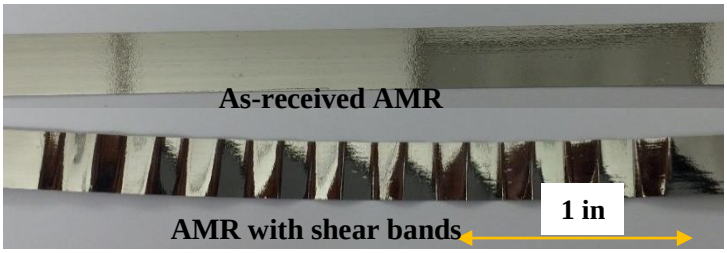

Figure 10 As-received and Shear Banded AMR used for corrosion testing.

fixture was generally used to produce an Amorphous Metal Honeycombs in what is called the "pin method". Each testing coupon contains about 14-16 bends as shown in Figure 10.

A procedure similar to tension testing of AMR was followed in order to evaluate the tensile properties of these shear band ribbons. This was to improve understanding of the effect of these shear bands have on the tensile mechanical properties of the metallic ribbon.

3.1.3 Testing of adhesives used for making "teardrop" honeycombs:

One of the most important factors governing the process of making a honeycomb lattice was the adhesive used to bond the material. As the aluminum honeycombs are typically made using an expansion method, [56] use of a slow curing adhesive is possible. But this AMH is made using a "bottom-up" approach. So it is essential to use an adhesive that can cure fast and also give the desired amount of strength. In this "bottom-up" approach, the metallic glass was bent with some plastic deformation (shear bands). So the adhesive has to with stand the reaction force of the bent ribbon.

The selected adhesive should possess strength at least greater than the force required to form a particular cell size. Another important factor governing the selection of adhesives was the chemical compatibility of the adhesive with the base material. In order to investigate this adhesive, shear and peel tests were performed. ASTM D1002 "Standard test method for apparent shear strength of single lap-joint adhesively bonded metal specimens by tension loading (Metal-to-Metal)," was followed for shear strength testing the adhesives used for making AMH. ASTM E865- 12 "Standard Specification for Structural Film Adhesives for Honeycomb Sandwich Panels" was used to test the peel strength of the adhesives.

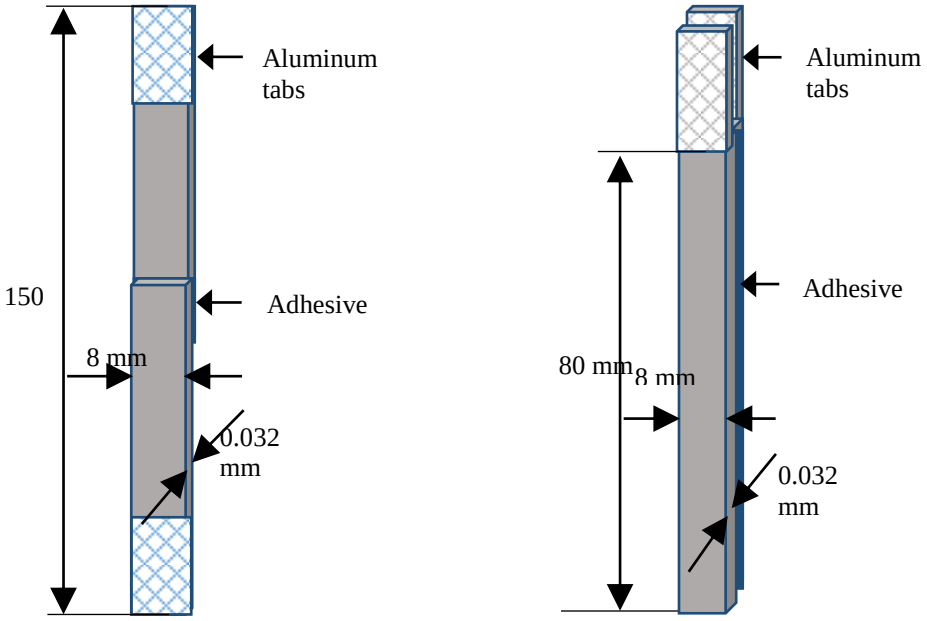

Figure 11 Sample preparation for Lap-joint shear test (left) and Peel strength test (right).

3.2 3.5% NaCl Immersion Corrosion Testing:

3.2.1 Testing apparatus:

The test was conducted in a closed environment. Para-film was utilized to cover any open portions of the beaker, and for holding the samples in place. An air pump was used for air saturating the electrolyte. A magnetic stirrer was employed for constant flow of oxygen to the sample surface. This ensured a consistent supply of oxygen to the metal surface. Samples were bent in a "U" shape and hung using acrylic sheets, zip ties and para-film. The apparatus is shown in Figure 12. Samples were bent in such a way that only 50 mm of each sample was exposed to the electrolyte. The unexposed portions of the ribbon help in gripping the sample.

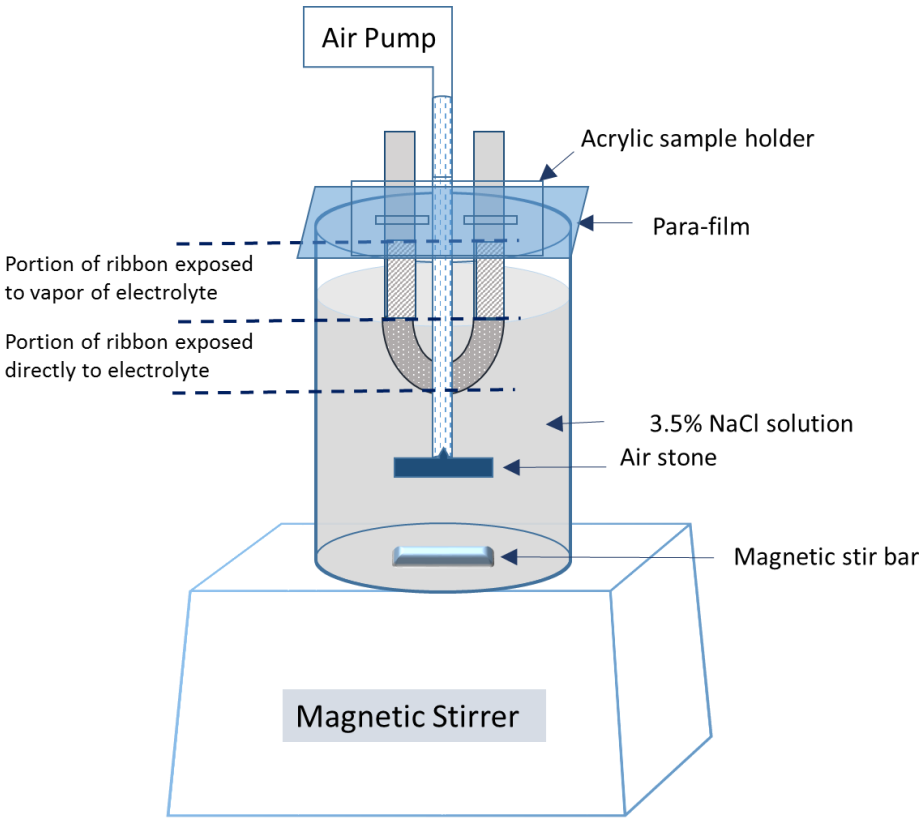

Figure 12 Set up for 3.5% NaCl corrosion testing.

3.2.2 Test Procedure:

Four types of samples were tested.

1. MB2826 Metallic glass ribbons in the as-received condition for evaluating the effect of corrosion on mechanical properties of the ribbon (AMR).
2. MB2826 Metallic glass ribbons in the as-received condition for evaluating the corrosiveness of the electrolyte (PIT).
3. MB2826 Metallic glass ribbons with shear bands (AMR with shear bands).
4. Commercial Aluminum 5052 honeycombs having density of 0.19 Mg/m^3, cell size of 3 mm (AlH).
5. Adhesive shear lap joints.

Duplicate (3 to 5) samples were tested. An electrolyte, 3.5% NaCl solution, was laboratory formulated using distilled water and lab grade sodium chloride. Samples were cleaned prior to testing by the "replicate cleaning procedure." Large poly-propylene beakers of 16 liter capacity were filled with the laboratory formulated 3.5% NaCl solution. For a constant supply of electrolyte (and oxygen) to the total surface area of the samples, the number of samples that can be tested depends on volume of electrolyte and exposed area of the sample. The number of samples can be evaluated using

$$Number\ of\ samples = 0.2\left(\frac{volume of\ electrolyte\ (ml)}{Exposed\ area of\ coupon\ (mm^2}\right)$$

Samples were mounted and Oxygen (air) was added to each beaker using an air pump and homogenized with a magnetic stirrer. At the completion of the test procedure, the beakers were left undisturbed.

3.2.3 Sample Cleaning and Mass Measurement:

Samples should be cleaned of corrosion products using a method that will not cause loss of the parent material. Mechanical brushing, cleaning with a solvent, and ultrasonic cleaning procedures are generally followed for efficient sample cleaning. ASTM G1-03 "Standard Practice for Preparing, Cleaning, and Evaluating Corrosion Test Specimens" explains a standard procedure, called the "replicate cleaning procedure," for cleaning the corroded samples. In this procedure, cleaning cycles are continued until a constant mass loss is observed. Cleaning cycle defines the basic steps followed for cleaning the corroded samples. For consistency in mass loss measurements, the same procedure was followed for cleaning the samples before and after corrosion.

*Sample Preparation before corrosion***:**

1. Rinse with water for 30 sec.
2. Clean using acetone and wipe off using Kim Wipes for 2 mins and note the mass measurement. (cleaning cycle).

3. Step 2 is repeated until there is consistency in the measurement of mass.

4. Air dry for 5 mins.

Preparation of corroded sample for weight loss investigation:

1. Rinse with tap water and wipe off using Kim wipes for 5 mins.

2. Mechanically clean both surfaces using brass and steel brushes.

3. Clean with acetone and wipe off using Kim wipes for 2 mins and note the mass measurement.

4. Step 2 is repeated until there is consistency in the measurement of mass.

5. Rinse with water for 60 sec, allow for air drying for 5 mins.

3.2.4 Calculation of Corrosion Rate and Penetration Rate:

Samples cleaned by the "replicate cleaning procedure" were weighed using an analytical balance with a 0.1 mg precision and 0.1 mg repeatability. ASTM G1-03 "Standard Practice for Preparing, Cleaning, and Evaluating Corrosion Test Specimens" was followed to calculate the corrosion rate and penetration rate from the measured mass loss and area of exposure.

Corrosion rate penetration depths were calculated using

$$\text{Corrosion rate (C. R)} = \frac{\text{K X W}}{\text{A X T X D}}$$

Error in corrosion rate, Δ (C. R) = (C .R) $[\frac{\Delta w}{w} + \frac{\Delta A}{A}]$

$$\text{Penetration rate (C. R)} = \frac{\text{C X W}}{\text{A X D}}$$

Error in penetration rate, Δ (P. R) = (P .R) $[\frac{\Delta w}{w} + \frac{\Delta A}{A}]$

Where

K = 87600 mm/y

C = 1 (constant corresponding to desired measuring unit, 1 for mm)

W = Mass loss (g)

A = Exposed area (sq. mm)

T = Time of exposure (hrs.)

D = Density of material (g/cc)

3.2.5 Planned Interval Testing (PIT):

Planned Interval Testing is a technique for evaluating the influence of time on corrosion of metals and time dependent variations in the corrosiveness of the environment. As the test progresses, variation in the corrosion rates can occur as a result of change in concentration of corrosive agents in the environment. Generally this testing involves exposure of multiple samples for different durations during the total time of testing. The durations are selected to obtain corrosion data for period of initial exposure, prolonged exposure, and a time period at the end of the longer exposure period. Comparison of the corrosion rates at different durations will help in assessing the corrosiveness of the electrolyte and metal corrodibility. In this testing procedure, a modified PIT has been employed. Over a period of 30 days, samples were changed every fifth day. The time of exposure for these PIT samples is 5 days. Corrosion and penetration rates were calculated based on mass loss. These rates were used to evaluate the corrodibility of the electrolyte and metal corrosiveness.

3.3 Salt Spray Test:

The salt spray procedure involves spraying of 5% NaCl salt solution on the samples being tested. Typically, samples are inserted in the temperature-controlled chamber and then salt solution is sprayed

on-to the samples as a fine fog mist. Samples are constantly subjected to corrosion, as the spray is continual and keeps the samples wet. Samples are frequently rotated with in the chamber to ensure that all the samples are exposed to salt spray mist as uniformly as possible. The test procedure was followed according to ASTM B117 "Standard Practice for Operating Salt Spray (Fog) Apparatus. "Salt spray chamber, sample preparation, and mounting the samples is shown in Figure 13

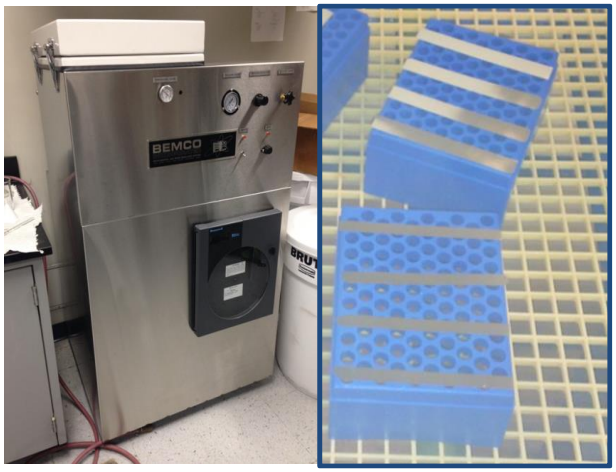

Figure 13 Set up for Salt Spray test along with sample preparation.

3.4 Mechanical Properties of corroded $Fe_{45}Ni_{45}Mo_7B_3$ ribbon:

Corroded MG ribbons are subjected to a tensile test to study the effect of corrosion on the mechanical properties. Similar testing procedure followed for as-received samples, explained in section 3.1.1 is followed for the corroded samples as well.

3.5 Measurement of Thickness of Corroded AMR:

Corrosion of AMR will result in a loss of parent material. As shown in Table 2 thickness is an important parameter in estimating the compressive strength of AMH. So a precise and accurate measuring technique is required. Here radiography was used to measure the change in thickness due to corrosion. For this purpose, an X-ray Micro CT was used. The basic principle is same as that of a medical

radiography. When penetrating radiation (X-rays in this case) is focused on a solid object, some of the radiation will be absorbed while some gets transmitted. The relative amounts depend on thickness and density of the object. The transmitted radiation deposited on a photographic film will result in an image of the object's internal structure. This image can be processed and quantitative intensity of the transmitted radiation can be obtained. As different thicknesses of same material will result in different intensities, measured intensities can be used to calculate the thickness of the ribbon. The interaction of X-rays with matter and the general relation between intensities and path length can be explained using Beer-Lambert's Law. According to this law, the physical properties of an object placed in the path of an X-ray are encoded in the attenuation coefficient (μ). For a given X-ray energy each material will have a characteristic attenuation coefficient that quantifies the tendency of an object to absorb or scatter. The basic assumptions associated with it are

1. No Refraction or Diffraction: The incident x-ray beams travel in straight lines and do not bend as they pass through the object.
2. X-rays are Monochromatic in nature: all the waves that make up the x-ray beam are of same frequency.

Here, the X-ray source in use is not monochromatic, but is polychromatic. That is, the waves that make up the X-ray beam are across a range of frequencies. This necessitates formulation of a relation between the measured intensities and path length (thickness of the object). Also the intensity of incident x-rays at the surface of the object depends on its surrounding environment. To account for this change, a bright field image is collected and the actual images are subtracted from it. An image collected without any object in the path of x-ray is called "Bright Field Image". By subtracting actual images from the bright field image and then processing the resulting image for intensities, we obtain absorbed intensities. Sample image collection is shown in Figure 14

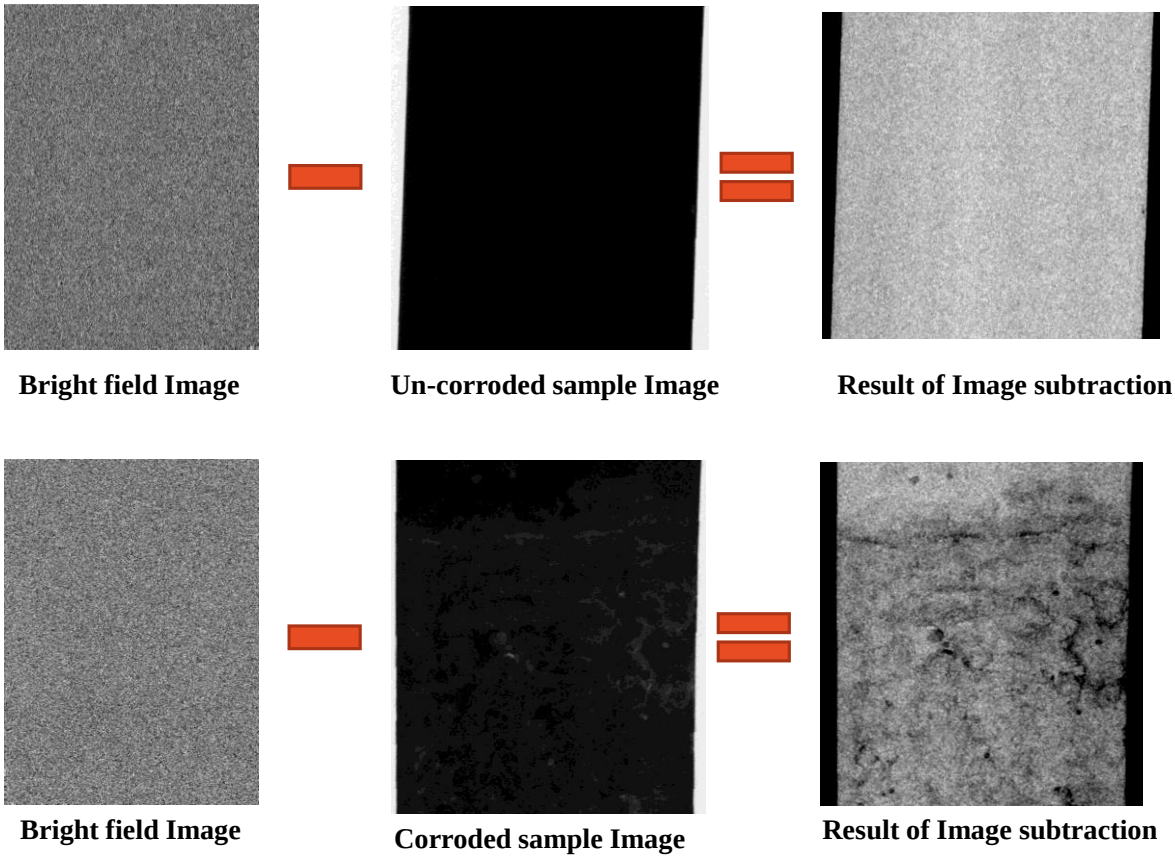

Figure 14 Image processing of un-corroded and corroded AMR radiographs.

To formulate an empirical relation between the absorbed intensities and thickness of sample, different thicknesses ranging from 18 to 99 microns were used. Due to the unavailability of AMR of different thicknesses, a single ribbon of 0.032 mm was rotated in 3 degree steps and the corresponding intensities were measured. In addition to this, some AMRs were polished down to obtain lower thicknesses (<0.032 mm). And double and triple thickness ribbons were also used. The thicknesses of AMR (ranging from 18 to 99 microns) were measured using a micrometer of resolution of 0.001 mm.

Absorbed intensities of the corroded ribbons was measured in a similar way and the above formulated relation was used to calculate the thickness of corroded Amorphous Metal Ribbons.

3.6 Compression of Aluminum and Amorphous Metal Honeycombs:

The thicknesses measured from radiography were used to predict the compressive strength of AMH. These predictions were then validated using experimental results. Experimental results were obtained by making an AMH from corroded "AMR with shear bands" and then compressing them. In case of Al-H, strength retention capacity is obtained by corroding Aluminum honeycombs and then compressing them. The empirical equations used to predict compressive strength due to elastic buckling $(\sigma_{el}^{*})_3$ of AMH and due to plastic buckling $(\sigma_{pl}^{*})_3$ of AL-H in the out-of-plane X_3 direction are given by

Table 4 Compressive axial strength of Amorphous Metal Honeycombs

Property	Amorphous Metal Honeycomb
Density $\left(\frac{\rho^*}{\rho_S}\right)$	$2.06\left(\frac{t}{r}\right)$
Compressive strength	$2.63E_s\left(\frac{\rho^*}{\rho_S}\right)^3$

CHAPTER IV

RESULTS

4.1 Planned Interval Test:

Over a period of 30 days, samples were changed every fifth day. The time of exposure for these PIT samples was 5 days corrosion and penetration rates were calculated based on mass loss. These rates were used to evaluate the corrodibility of the electrolyte and metal corrosiveness.

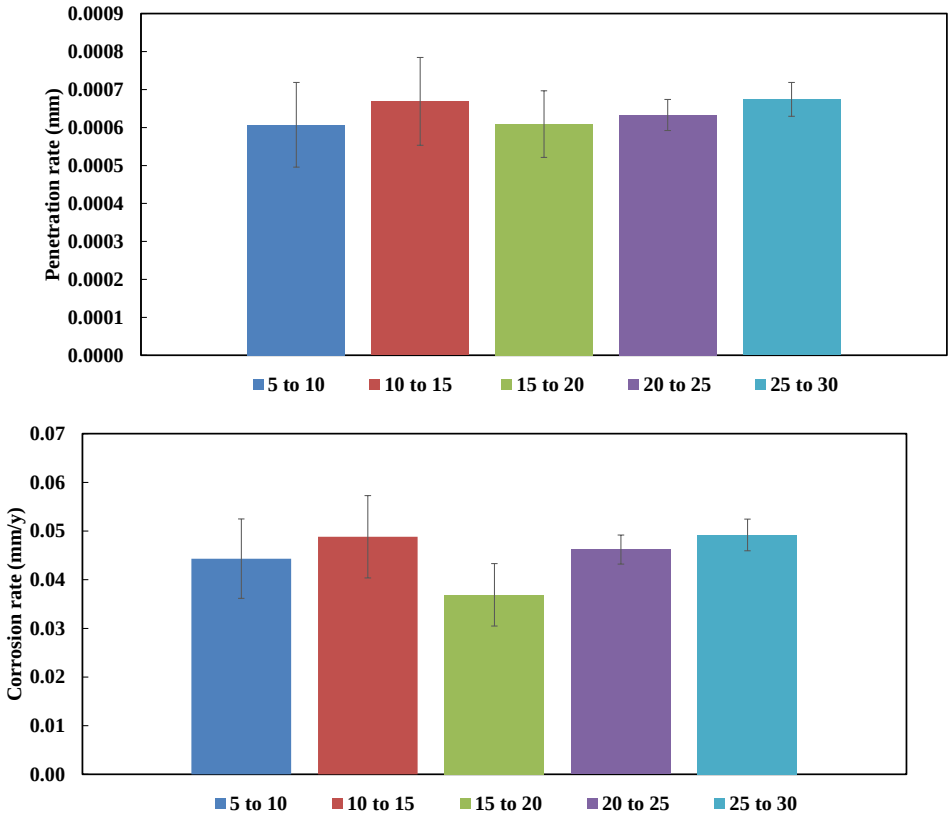

Figure 15 Penetration depth and corrosion rate results from PIT.

4.2 Mass Loss and Corrosion Rate measurements of AMR:

Amorphous Metal Ribbons in an as-received condition were tested for corrosion in NaCl environments, namely 3.5% NaCl, Salt Spray, and Linear Polarization Resistance. The mass loss (%) and corrosion rate (CR) measurements are plotted as a function of time of exposure

Table 5 Corrosion Rates (CR) of AMR from all three different NaCl environments

CR from 30 days salt spray *(mm/y)	Saturated CR from 3.5% NaCl *(mm/y)	CR from 5.8% NaCl Linear polarization measurements (mm/y)
0.03	0.03 ± 0.01	0.02 ± 0.01

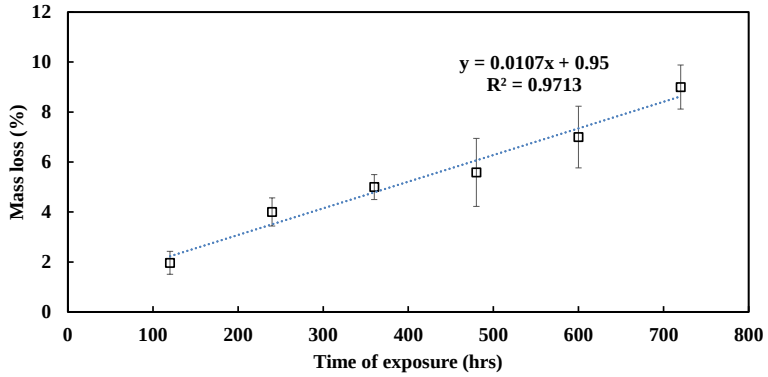

Figure 16 Corrosion rate of AMR in 3.5% NaCl and Salt Spray as function of time of exposure.

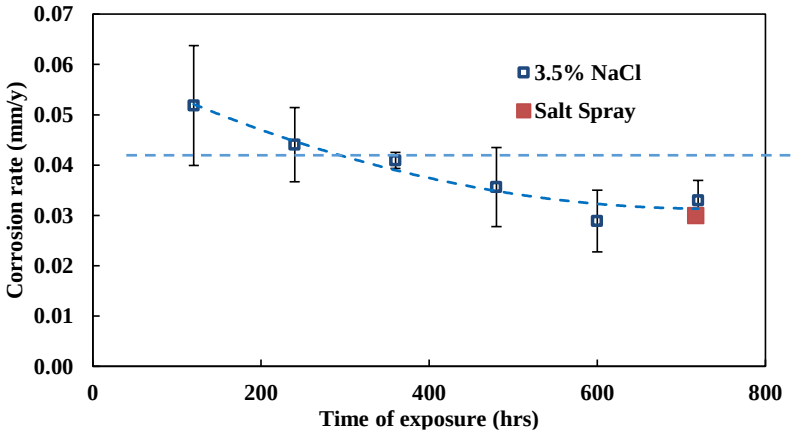

Figure 17 Mass loss (%) of AMR as s function of time of exposure with a linear trend line.

*Calculation of number of significant digits in corrosion rate are included in Appendix-I

4.3 Effect of Corrosion on Mechanical Properties of AMR:

Over an exposure period of 30 days, the maximum load carrying capacity and Young's modulus of AMR were calculated from tension tests.

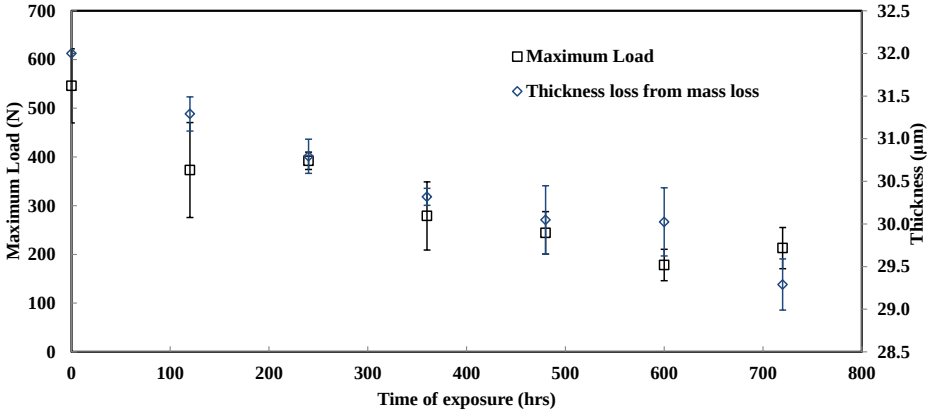

Figure 18 Load carrying capacity and thickness from mass loss of as-received AMR as a function of time of exposure.

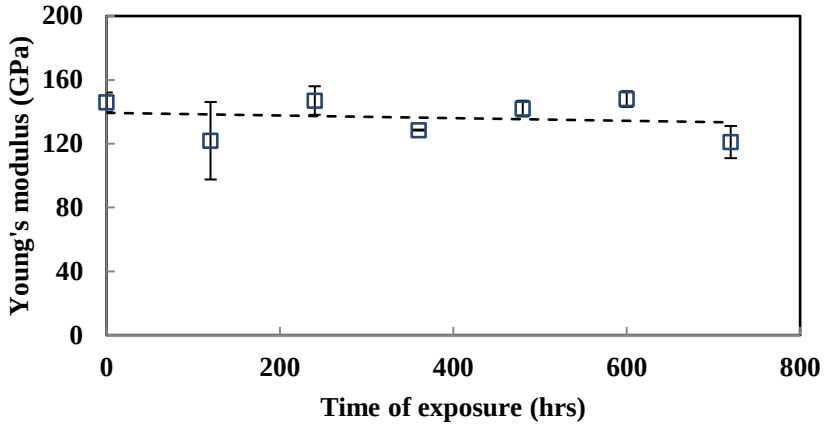

Figure 19 Plot showing change in Young's modulus of as-received AMR as a function of time of exposure.

4.4 Thickness loss from Mass loss of AMR:

Loss in thickness of corroded AMR is calculated using measured mass loss as a function of time of exposure.

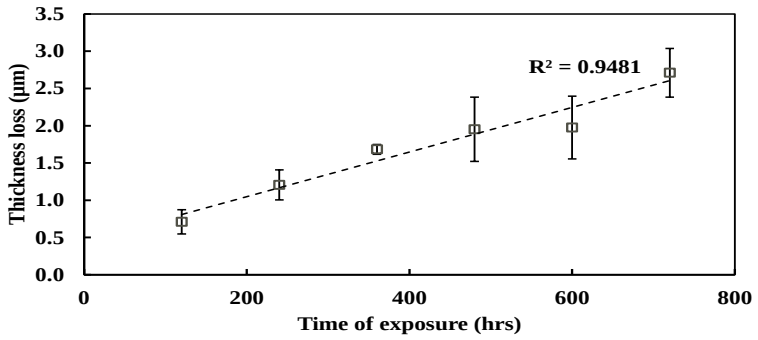

Figure 20 Thickness loss calculated from mass loss of as-received AMR as a function of time of exposure.

4.5 Thickness loss in AMR using Radiography:

An empirical relation between intensity and path length (thickness of sample) was formulated to calculate the effective thickness of the corroded AMR. Experimentally calculated intensities was plotted as a function of corresponding measured thickness values. The empirical relation formed is

$$\text{Intensity} = -0.0019*(t^4) + 0.5474*(t^3) - 58.97*(t^2) + 2826.3*(t)$$

Where, t is the thickness of AMR, Intensity is the absorbed intensity.

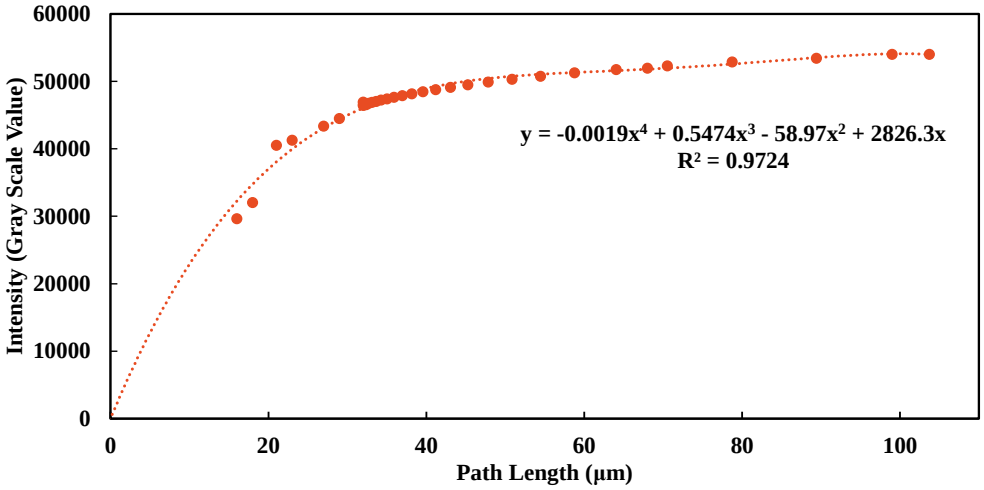

Figure 21 Formulation of empirical relation between measured intensities and path length (thickness of material).

Then intensities of the corroded AMR were measured, and corresponding thicknesses were calculated from the above empirical relation. Histograms of corroded AMR were collected*. Mean intensities (intensities corresponding to maximum frequency) from the histograms were used to calculate the thickness of the corroded AMR.

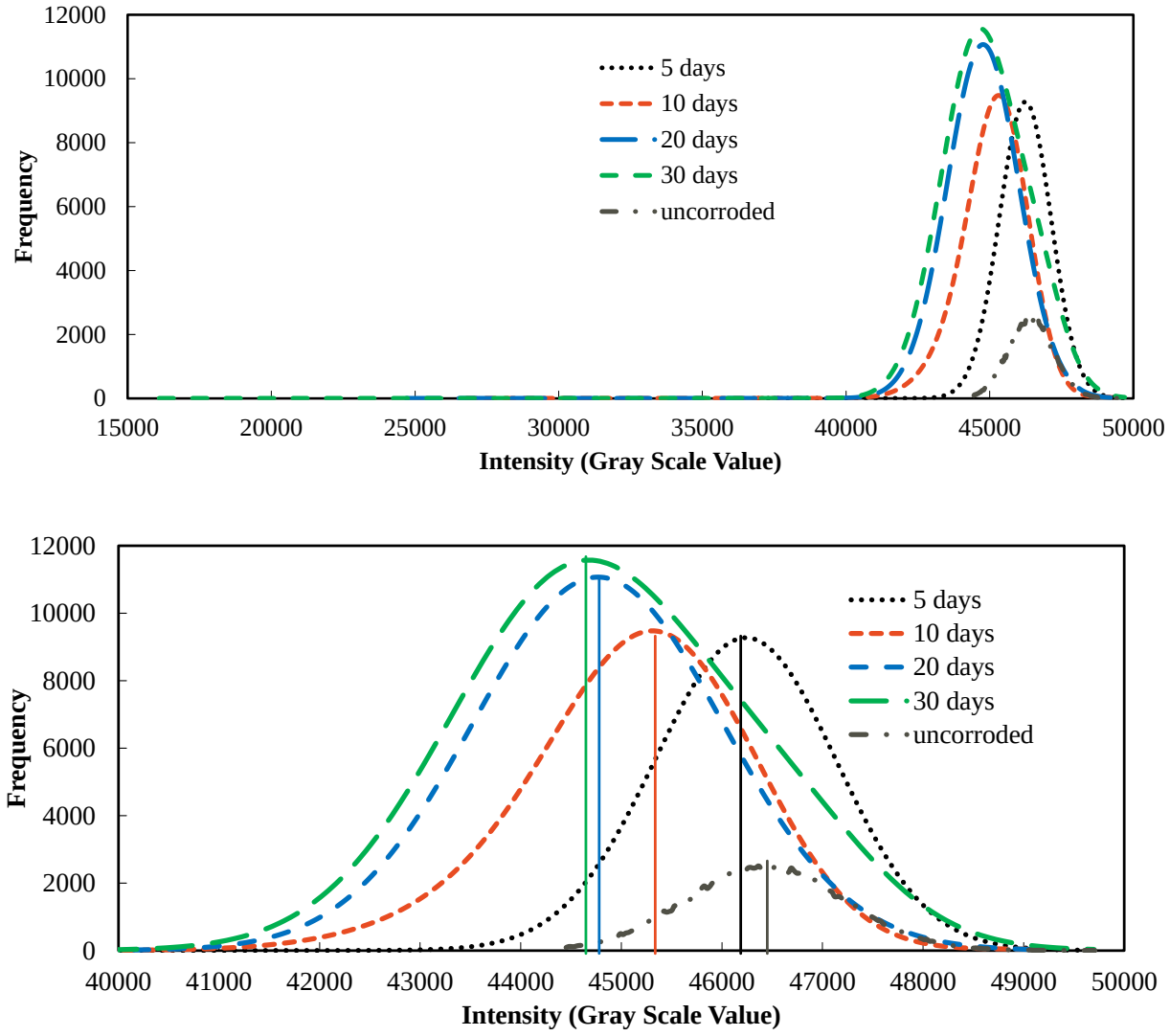

Figure 22 Histograms of un-corroded and corroded as-received AMR with peaks indicated.

*Using ImageJ and MATLAB

Table 6 Thickness from mean intensities, minimum intensities, and mass loss as a function of time of exposure

Time of exposure (hrs)	Mean thickness (µm)	Min thickness (µm)	Thickness from mass loss (µm)	Stdev (µm)
0	32	32	32	1
120	32	20	31	0.2
240	31	12	31	0.2
480	30	11	30	0.1
720	29	7	29	0.4

Comparison of thickness calculated from radiography and mass loss are plotted as a function of time of exposure.

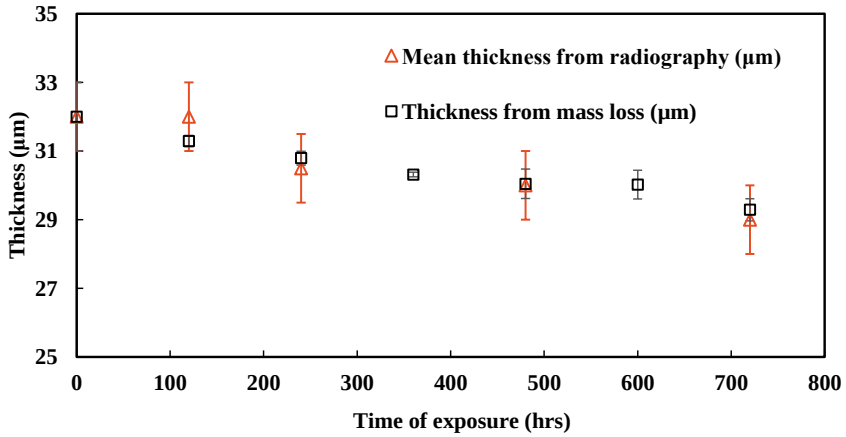

Figure 23 Comparison of thickness calculated from radiography and measured mass loss as a function of time of exposure.

4.6 Compressive strength of Amorphous Metal Honeycombs:

Thickness calculated from above was used to predict the compressive strength of AMH. The predicted values were then compared with experimental compressive strength results.

Table 7 Compressive strength of AMH predicted from radiography and experiments, effective thickness calculated from experimental values

Time of exposure (hrs)	Predicted compressive strength corresponding to Mean thickness(MPa)	Error (MPa)	Experimental compressive strength (MPa)	Error (MPa)	Effective thickness from experimental strength (µm)	Error (µm)
720	20	2.1	17	1.8	27	1
480	22	2.2	21	2.2	29	1
240	24	2.4	23	2.4	30	1

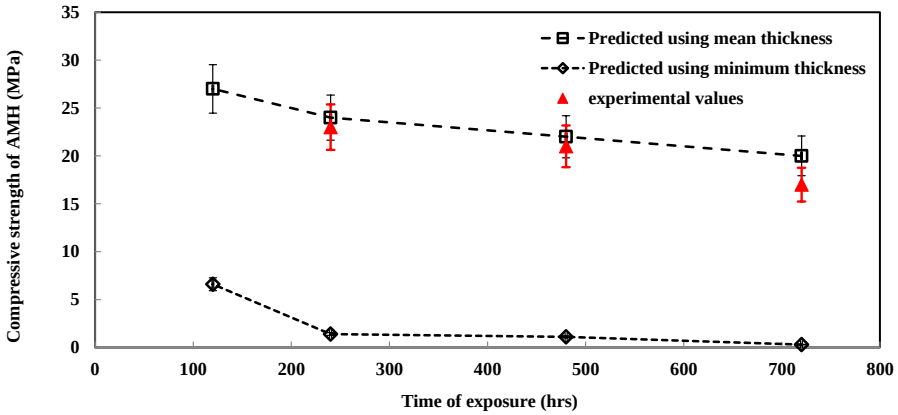

Figure 24 Comparison of compressive strengths predicted from mean thickness, minimum thickness, and experimental results.

4.7 Compressive strength of Aluminum Honeycombs:

Aluminum honeycombs were corroded for different time periods (multiples of 5 days) and then compressed to observe changes in their compressive behavior. Peak and crush strengths were calculated from the compression data.

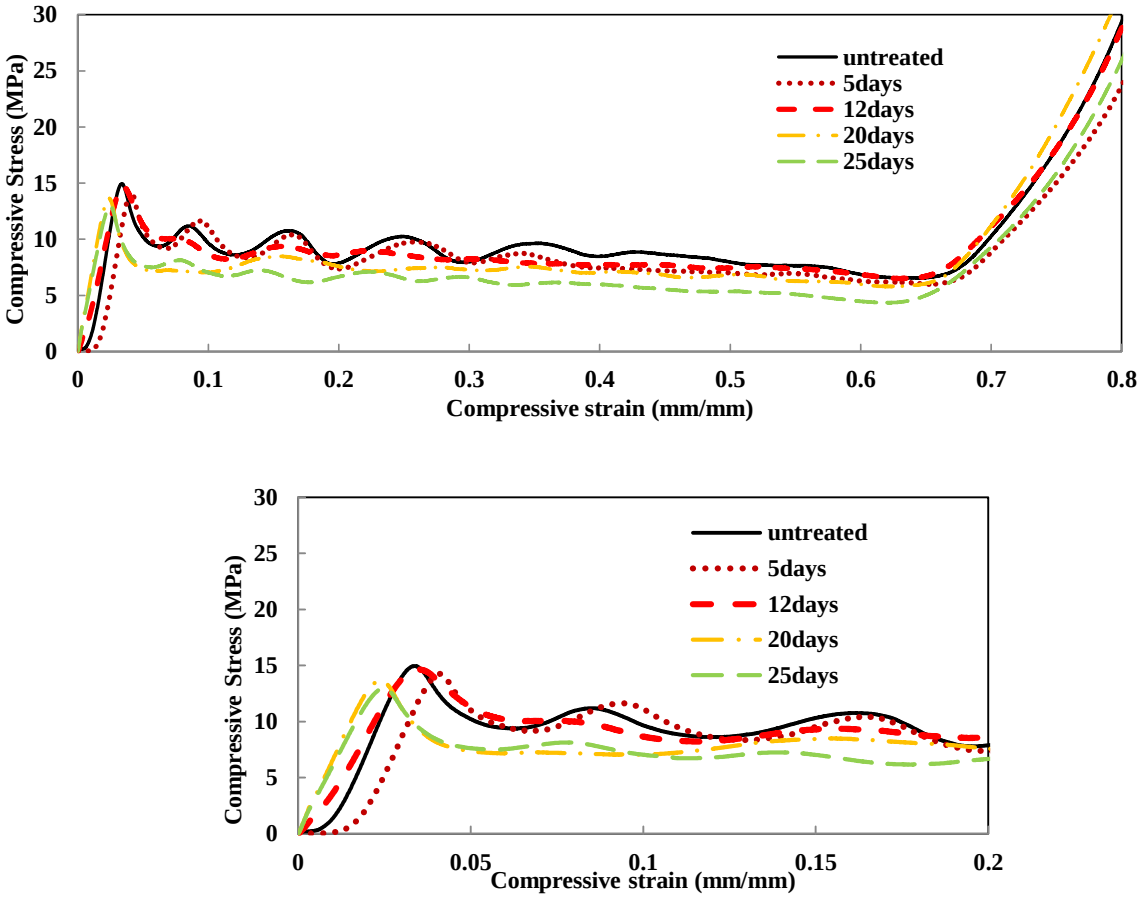

Figure 25 Graphs showing the peak strength (left) and crush strength (right) as a function of time of exposure.

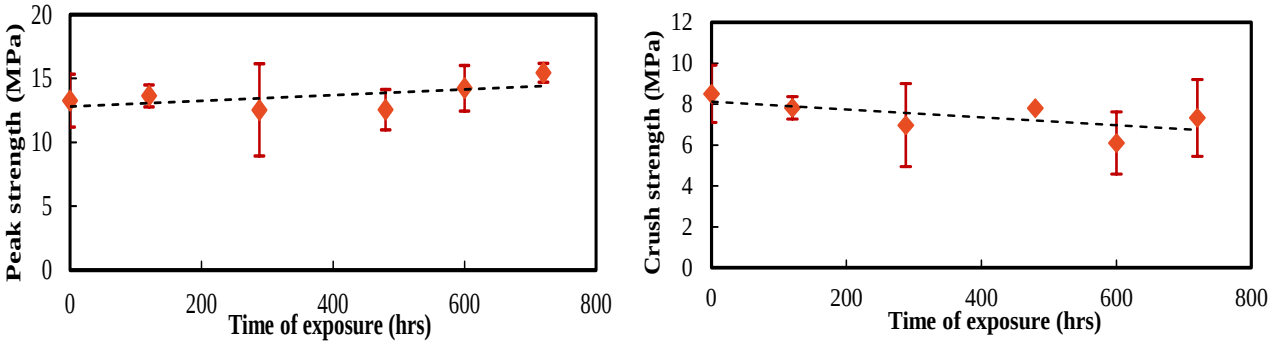

Figure 26 Compressive stress-strain curves of corroded and un-corroded Al-H highlighting the plateau region.

4.8 Compressive Strength retention capacity of Al-H and AMH:

Strength loss (%) as a function of time of exposure was calculated. Both peak and crush strengths of Al-H and only peak strengths of AMH are reported. Because of the weak inter-cellular bonds in AMH, it is difficult to exactly calculate the crush (plateau) strength.

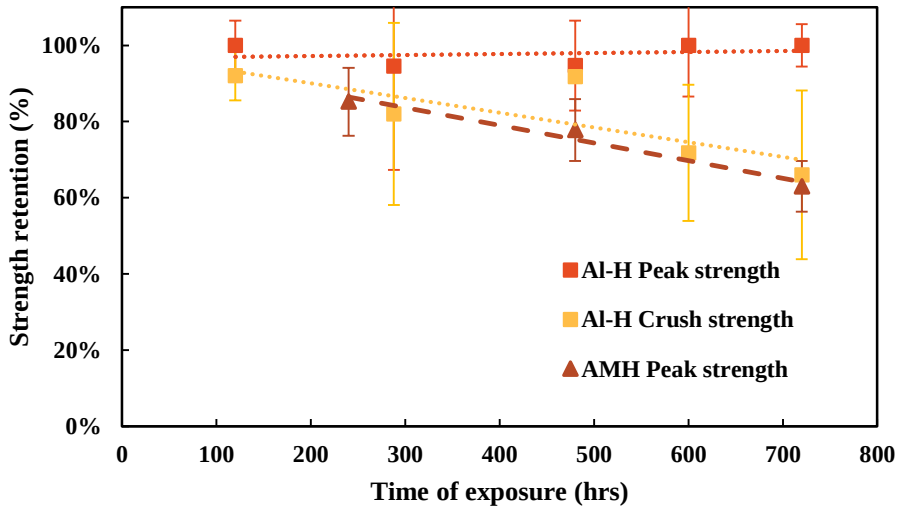

Figure 27 Comparison of strength retention capacity of Al-H and AMH as a function of time of exposure.

4.9 Effect of Shear Bands:

Results of bending testing showing the critical cell size for the formation of shear bands is shown.in Figure 27

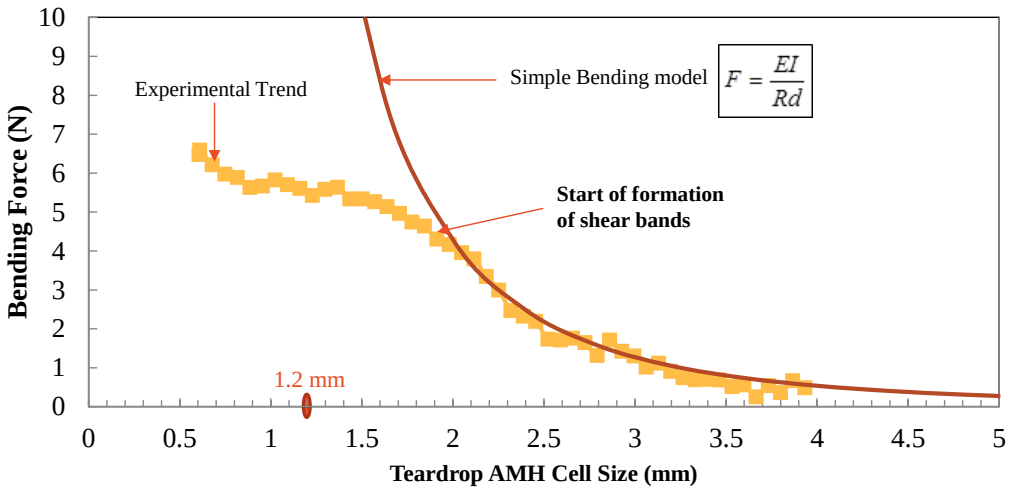

Figure 28 Plot showing the critical cell size for formation of shear bands highlighting the cell size used in this thesis.

Effect of shear bands on the Young's modulus of AMR is shown.

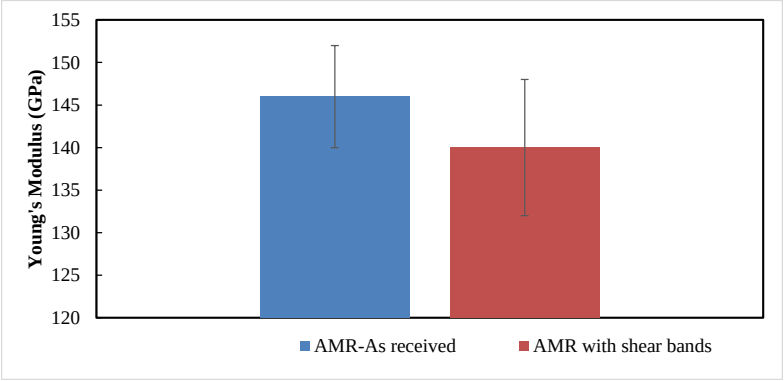

Figure 29 Comparison of Young's modulus of as-received AMR and AMR with shear bands.

Shear bands affected the rate of the dissolution of elements. Mass loss (%) and the corresponding Corrosion Rate (CR) as function of time of exposure and in comparison with as received AMR is shown Figure 30.

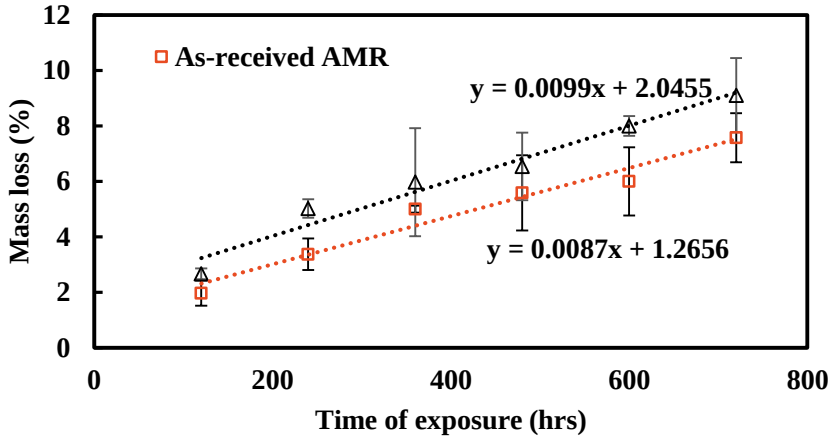

Figure 30 Comparison of Mass loss (%) of as-received AMR and AMR with shear bands highlighting slope of the trend line equations.

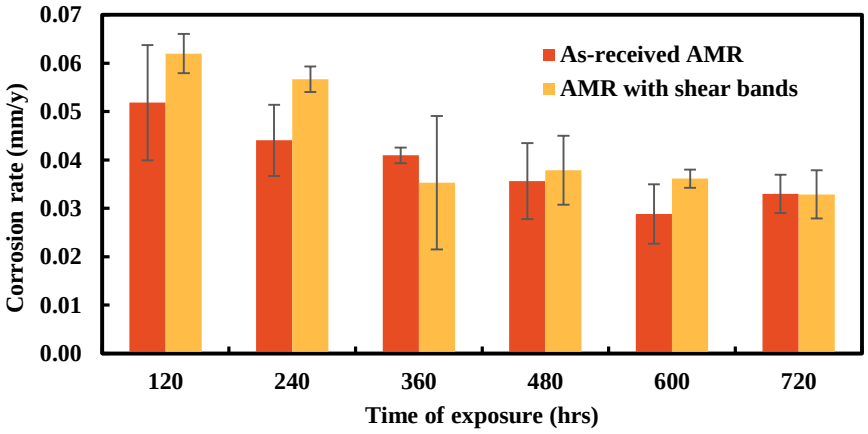

Figure 31 Comparison of corrosion rates (CR) of as-receive and shear banded AMR.

The effect of shear bands on the strength carrying capacity and Young's modulus of AMR in comparison with as-received AMR is plotted as a function of time of exposure below

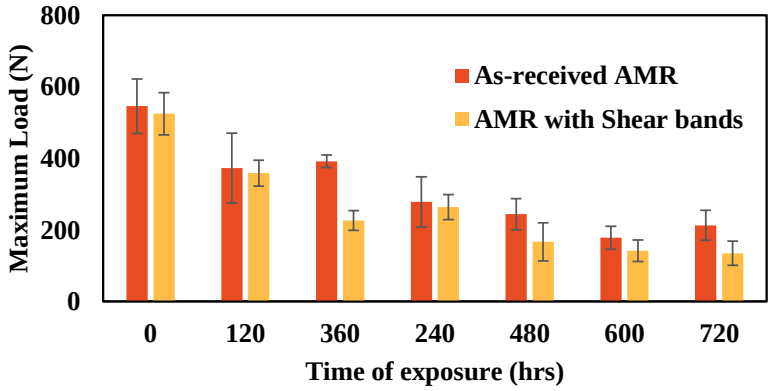

Figure 32 Load carrying capacity of AMR with shear bands in comparison with as-received AMR as a function of time of exposure.

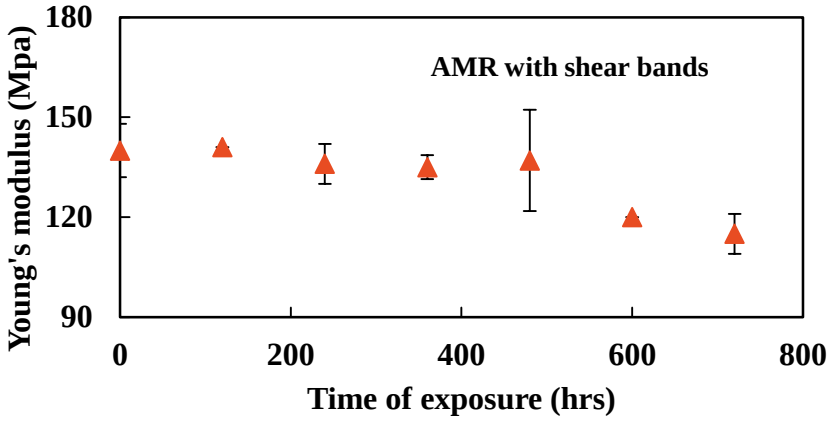

Figure 33 Change in Young's modulus of AMR with shear bands as a function of time of exposure.

To estimate the effect of shear bands on the compressive strength of AMH, a study of the effect of shear bands on the loss of thickness due to corrosion is important. Thickness calculated from mass loss of AMR with shear bands in comparison with as-received AMR were plotted as a function of time of exposure.

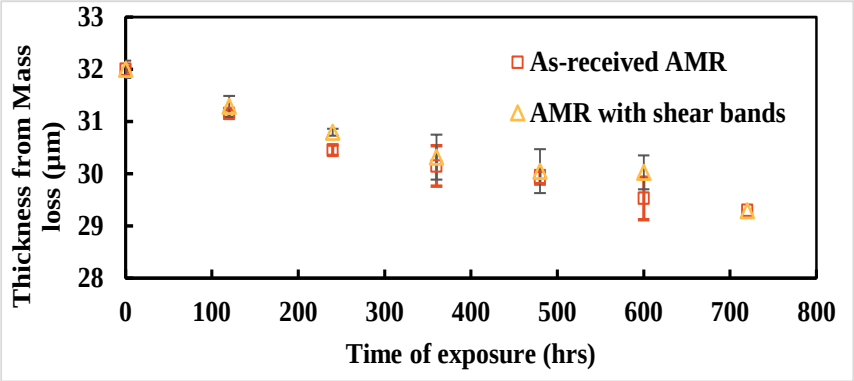

Figure 34 Comparison of thickness loss from mass loss of AMR with shear bands and as-received AMR as a function of time of exposure.

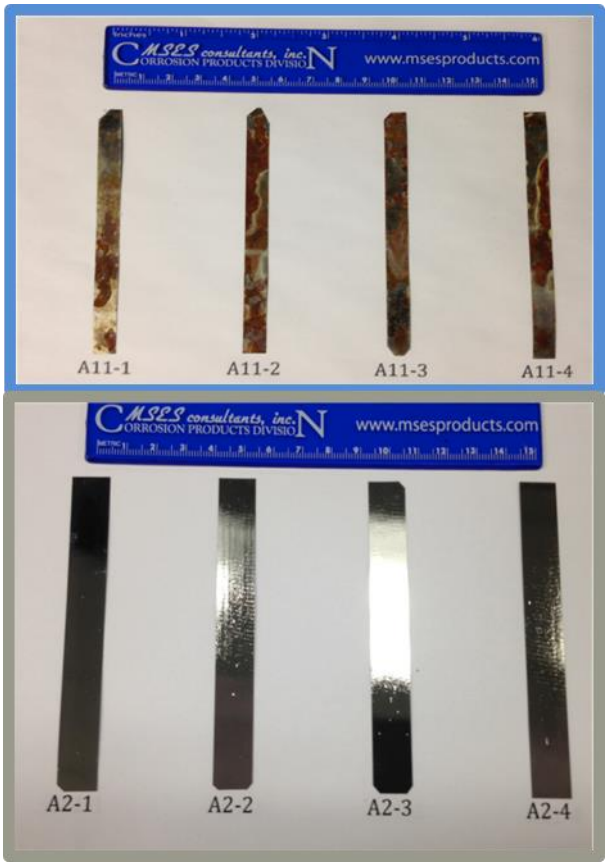

Figure 35 Comparison of Fe-Ni and Fe-Cr based metallic glass after 717 hrs of exposure to salt spray.

CHAPTER V

DISCUSSION

5.1 Planned Interval Test:

From results of the Planned Interval Test (PIT), it can be seen that the penetration depth and corrosion rate of the as-received AMR for time periods 5-10 days, 10-15 days, 15-20 days, 20-25 days, 25-30 days are equal to within the experimental error as shown in Figure 15. This shows that the corrosiveness of the electrolyte remains unchanged [54] during the test period of 30 days (720 hours).

5.2 Mass Loss and Corrosion Rate measurements of AMR:

When an Iron containing specimen is exposed to a neutral (6-8 pH range) environment, the following electrochemical reactions takes place [55].

$$\mathrm{Fe} \leftrightarrow \mathrm{Fe}^{2+} + 2\mathrm{e}^{-1} \text{ (oxidation)}$$

$$\frac{1}{2}\mathrm{O}_2 + \mathrm{H}_2\mathrm{O} + 2\mathrm{e}^{-1} \leftrightarrow 2\mathrm{OH}^{-1} \text{ (reduction)}$$

$$..... + 2\mathrm{OH}^{-1} \rightarrow \alpha - \mathrm{FeOOH}(\textit{rust}) + \mathrm{etc.}$$

Experimental Environments, i.e., 3.5% NaCl, Salt Spray, 5.8% NaCl polarization tests were done in a pH range of 6-8. In such neutral environments, the amount of dissolved oxygen (DO) present in the electrolyte determines the rate of the reaction. Also thr % Mass loss varies linearly with time of exposure Figure 17 in the tested regime of 0-30 days. This shows that the corrosion reaction is following "First-Order Kinetics". In a first-order reaction, rate is proportional to concentration of one of the reactants [56]. Therefore,

Rate = k [DO] where k is a constant

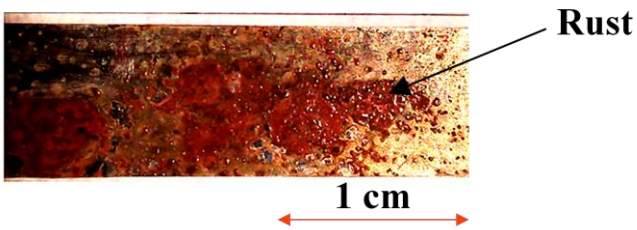

Figure 36 Corroded AMR showing signs of rust.

According to first-order kinetics, corrosion rate, defined as rate of loss of material, should be constant. This is in agreement with the calculated corrosion rates from all three environments as shown in Table 5. Corrosion rates from 3.5% NaCl immersion test are initially high before they started saturating. Higher corrosion rates are observed initially during the process of stabilization of the amount of dissolved oxygen in the electrolyte. i.e. until the

Amount of oxygen supplied externally = amount of oxygen consumed from the electrolyte

Oxygen is consumed either in the corrosion reaction or in formation of equilibrium between the surface of electrolyte and air inside the closed chamber. Also the formula used to calculate corrosion rate is applicable only for uniform corrosion. But a localized corrosion pattern is observed in AMR. Therefore, calculated corrosion is an approximation.

5.3 Effects of Corrosion on Mechanical Properties of AMR:

Material loss due to corrosion resulted in reduction of cross-sectional area, which affected the load carrying capacity of AMR. No change in width of the ribbon was observed. This shows that all the material loss is from thickness. Also the maximum load carrying capacity followed the same trend with respect to time of exposure as thickness loss calculated from mass loss (figure). Young's modulus (E_s), which is a material property, did not changed significantly during the 30 days of testing, as shown in Figure 19.

5.4 Thickness loss from Mass loss of AMR:

Thickness loss calculated from mass loss, as shown in Figure 20, followed the same trend as mass loss (%). This is expected as the equation used for calculating thickness loss from measured mass loss is

$$M = \rho x V = \rho x (A x t)$$
$$\Rightarrow \Delta t = \frac{\Delta M}{(\rho x A)}$$

Where

M is mass of specimen (g)

ρ is density of specimen (Mg/m^3)

V is volume of specimen (cm^3)

A is surface area (cm^2)

t is thickness of specimen (cm)

Use of this equation to calculate thickness loss involves the following assumptions.

1. All mass loss due to corrosion can be accounted from thickness loss in the specimen after corrosion.

2. *Corrosion is uniform over the exposed surface of the specimen.*

Visual and microscopic inspection of the corroded samples indicated a strong localization of the corrosion. This shows that the calculated thickness using the above equation is approximate. This limits usage of these values and requires a more appropriate way of measuring thickness loss.

5.5 Thickness loss in AMR using Radiography:

The polychromatic X-ray source and corresponding non-linearly varying attenuation coefficient of AMR necessitated the formulation of an empirical relation between the intensities and measured thicknesses. From Figure 21, we can see that the rate of change of intensity for a finite change in path length (thickness) is higher at lower thicknesses and decreases as the path length increases. This is evident from the fourth order polynomial equation passing through the origin. A fitted trend line resulted in a deviation from experimental values at lower path lengths. This can be due to error in the micrometer used to measure thicknesses. The micrometer measures thickness on an area. Thickness of the polished AMR (corresponding to lower path lengths) was first measured with the micrometer, the lower thickness areas were marked, and then the same regions were radiographed. An error is possible in this process. This error also contributes to the observed deviation.

From Figure 22, it is evident that the intensities of corroded AMR ranged from 15000 to 50000. On a thickness scale, this range corresponds to 0.007 mm to 0.032 mm. Error associated with this conversion is 0.001 mm. This error is calculated from an un-corroded AMR. For an un-corroded AMR, intensities range from 46900 to 49600. The standard deviation of 2700 corresponds to a thickness of 0.001 mm. The same amount of standard deviation was also observed in the measurement of un-corroded AMR using the micrometer. From the histograms of corroded ribbons, it can be seen that the mean intensities decreased with increase in time of exposure from 0 to 30

days. This shows that corrosion resulted in a decrease of thickness and this decrease in thickness increases with increase in exposure time. From Table 6, we can observe that with increase in exposure time from 0 to 720 hours (30 days), mean thickness decreased from 0.032 to 0.029 mm, while minimum thickness has decreased from 0.032 to 0.007 mm. This shows that there is a localization of corrosion and this localized attack has increased with increase in exposure time. In one of the corroded samples (620 hours), this localization resulted in a through hole as shown Figure 37

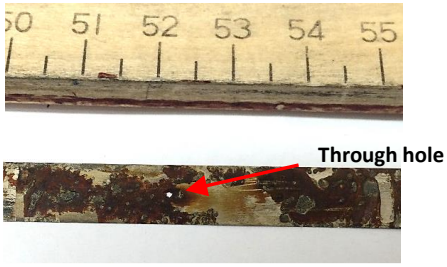

Figure 37 Through hole observed in 620 hours corroded AMR sample

Mean thicknesses (T_1) calculated from radiography are in agreement with thicknesses (T_2) calculated from mass loss as shown in Figure 23. T_1 is varied from T_2 initially at smaller exposure times but the agreement increased with increase in time of exposure. This shows that corrosion started as localized and propagated non-uniformly over the total surface area of exposed AMR.

5.6 Compressive strength of Amorphous Metal Honeycombs (AMH):

The effect of corrosion on compressive strength of AMH was studied stepwise. Changes in different parameters in compressive strength were first estimated from different tests. Then these changes as a function of time of exposure were used to predict the compressive strength of AMH. The mean thickness from radiography (T_1) and change in Young's modulus using tension testing. Young's modulus (E_s) did not change over the testing period of 30 days. But the thickness of the AMR changed by a considerable amount. This shows that the reduction in compressive strength of AMH can be associated with the change in thickness of AMR. The mean thickness from radiography (T1) for different time periods was used to estimate the change in compressive strength of AMH. Figure

24 compares the estimated and experimentally evaluated compressive strengths. Alongside, compressive strengths predicted using minimum thicknesses are also shown. The corresponding values are tabulated in Table 7. This shows that the experimental values are in agreement with predictions using mean thicknesses, not the minimum.

5.7 Compressive strength of Aluminum Honeycombs (Al-H):

CR-PAA coated Aluminum honeycombs were exposed to 3.5% NaCl for different time periods ranging from 0 to 30 days and then compressed. Figure 26 shows that there is no significant change in peak strength of the Al-H. But a change in the plateau behavior was observed. The number of undulations in the plateau region decreased with increase in time of exposure. Undulations represent the successive plastic folding of cell walls. This affected the crush strength of Al-H. A decrease in crush strength was observed as a function of time of exposure. Coatings helped in corrosion resistance behavior of Al-H at least until 720 hours of exposure to 3.5% NaCl.

5.8 Compressive Strength retention capacity of Al-H and AMH:

Figure 27 shows the comparison of strength retention capacities of Al-H and AMH. Peak and crush strengths are plotted in the case of Al-H but only Peak strengths are plotted in the case of AMH. Calculation of crush strength in case of AMH was not possible due to relatively weak intercellular bonding, which is typical for laboratory manufacturing of samples. In comparison, Al-H exhibited a better compressive peak strength retention capacity than AMH. Al-H retained almost 100% of its peak strength while AMH showed a decreasing trend with respect to time of exposure.

5.9 Effect of Shear Bands:

As mentioned earlier, not all AMH cell sizes will result in the formation of shear bands. There is a critical cell size below which shear bands are formed, which is about 1.9 mm in AMH. As shown in Figure 28, this cell size corresponds to the point where the experimental bending trend deviates from the simple bending model. The simple bending model corresponds to the bending formula (elastic bending). Deviation represents the start of formation of non-linear deformation from shear bands.

This corresponds to plastic bending, indicating that with formation of shear bands smaller cell sizes can be formed with lower bending forces. The 1.2 mm cell size, which is experimented here, falls in the shear band deformation regime

Figure 33 shows that there is no significant change in Young's modulus of AMR due to shear bands. This indicates that shear bands were not so significant to affect the elastic properties of the AMR. But they did change the corrosion behavior of AMR.

Initiation of shear bands requires more energy than initiation of dislocation slipping in conventional metals [1]. When exposed to corrosive environments, these high energy regions are more susceptible to corrosion than non-shear band regions of the ribbon forming a galvanic cell. Shear bands accelerate the rate of dissolution of elements. This resulted in an increased mass loss when compared to non-shear banded AMR. The higher slope of the trend line indicates that there is an increase in rate of mass loss as well. A similar trend is seen in corrosion rates. Initially corrosion rates of shear banded AMR were high when compared to as-received AMR. But as time progresses, they reach a similar equilibrium corrosion rate.

Shear bands formed by bending AMR over a 1.2 mm diameter pin resulted in a decrease of load carrying capacity. Reduction in strength is more evident at higher exposure times. A significant change in Young's modulus was not observed during the exposure period of 30 days. Though mass loss increased, there is no significant change in thickness loss calculated from mass loss of shear banded AMR when compared to as-received AMR. So there is no additional loss of compressive strength of 1.2 mm cell-size AMH due to shear bands.

5.10 Comparison of Fe-Ni and Fe-Cr based metallic glasses:

From Figure 35 it can be seen that the Fe-Cr did not show any signs of corrosion after 717 hrs of exposure to salt spray environment while the Fe-Ni alloy has shown rusting and a corresponding mass loss.

CHAPTER VI

CONCLUSIONS

- The amorphous structure, by itself, is not sufficient to engender better corrosion resistance than crystalline counterparts. Alloy composition is an important factor in comparing two metallic glasses or a metallic glass and a crystalline material. Fe-Cr based metallic glass has shown superior corrosion resistance than Fe-Ni based metallic glass.
- Corrosion in 3.5% NaCl resulted in deterioration of the compressive strength of AMH by 30% while not significant change is observed in case of Al-H in 30 days of continuous exposure. In this regard, CR-PAA coated commercial Al-H exhibited better corrosion performance than laboratory made Fe-Ni based AMH. Manufacturing defects and intercellular bonding play a role in this performance.
- Radiography was effective in estimating the thickness loss and thus the compressive strength of AMH. This can be extended to other material systems and related corrosion problems.
- Shear bands resulted from making 1.2 mm size cells in AMH and increased the mass loss, corrosion rate, and strength loss but did not affect the compressive strength of AMH

REFERENCES

1. Russell, A.J. and Ferguson, J.S. (January 1995). "Composite Repair Issues on the CF-18 Aircraft", Composite Repair of Military Structures, AGARD-CP-550, Neuilly-sur-Seine, France

2. Radtke, T.C. et al. (September 1999). "Hot/Wet Environmental Degradation of Honeycomb Sandwich Structure Representative of F/A-18: Flatwise Tension Strength", DSTO-TR-0908, 30 pgs

3. Granville, D.M. (1987). "Moisture Effects and Peel Testing of Polymethacrylimide Foam and Honeycomb Core in Sandwich/Skin Structures", Proceedings Fifth International Joint Military/Government-Industry Symposium on Structural Adhesive Bonding at U.S. Army Armament Research Development, and Engineering Center, American Defence Preparedness Association, Washington, D.C., pp. 224-230.

4. Campbell F. C., "The case against honeycomb core," Proc. International SAMPE Symposium and Exhibition, 49, 3680-3688 (2004).

5. Davis, J.R. (August 1999). Corrosion of Aluminum and Aluminum Alloys, ASM International, Materials Park (OH), 313 pgs.

6. Davis, Joseph R., ed. *Corrosion: Understanding the basics*. ASM International, 2000.

7. S.C. Dexter, Corrosion in Seawater, *Corrosion: Environments and Industries*, Vol 13C, *ASM Handbook*, ASM International, 2006, p 27–41

8. Chen, M. (2008). "Mechanical Behavior of Metallic Glasses: Microscopic Understanding of Strength and Ductility." Annual Review of Materials Research 38(1): 445-469.

9. Ashby, M. F. and A. L. Greer (2006). "Metallic glasses as structural materials." Scripta Materialia 54(3): 321-326.

10. W. L. Johnson and K. Samwer, "A universal criterion for plastic yielding of metallic glasses with a (T/T-g)(2/3) temperature dependence," *Physical Review Letters*, vol. 95, Nov 2005

11. Jayakumar, Balaji, and Jay C. Hanan. "Modeling the Axial Mechanical Response of Amorphous Fe45Ni45Mo7B3 Honeycombs." *Metallurgical and Materials Transactions A* 43.8 (2012): 2669-2675.

12. Fogarty JH. 2010 Honeycomb Core and the Myths of Moisture Ingression. Appl Compos Mater. 17:293-307

13. Gintert, L., Singleton, M., Powell, W.: Corrosion control for aluminum honeycomb sandwich structures, 33 rd international society for the advancement of manufacturing and process engineering (SAMPE) Technical Conference, Seattle, WA, November (2001)

14. Shafizadeh, J., Seferis, J., Chesmar, E., Geyer, R.: Evaluation of the in-service performance behavior of honeycomb composite sandwich structures. J. Mater. Eng. Perform. **8**(6), 661–668 (1999)

15. Shafizadeh, J., Seferis, J.: The effects of long time water exposure on the durability of honeycomb cores, 45th international society for the advancement of manufacturing and process engineering (SAMPE) Symposium, Long Beach, CA (May 2000)

16. Li, C., Ueno, R., Lefebvre, V.: Investigation of moisture ingress and migration mechanisms of an aircraft rudder composites sandwich structure, 38th international society for the advancement of manufacturing and process engineering (SAMPE) Technical Conference, Dallas (November 2006)

17. Whitehead, S., McDonald, M., Bartholomeusz, R.: Loading degradation, and repair of F-111 bonded honeycomb sandwich panels—a preliminary study, Australian Defense Science and Technology Organization (DSTO) Report DSTO-TR-1041 (August 2000)

18. Dong-Mei Wang, Z.-W. W., Qiang-Hua Liao, (2009). "Energy absorption diagrams of paper honeycomb sandwich structures." Packaging Technology and Science 22(2): 63-67.

19. Duwez, Pol. "Metastable phases obtained by rapid quenching from the liquid state." *Progress in Solid State Chemistry* 3 (1967): 377-406.

20. Scully, John R., A. Gebert, and Joe H. Payer. "Corrosion and related mechanical properties of bulk metallic glasses." *J. Mater. Res* 22.2 (2007): 302-313.

21. Schultz, L. (1988). "Formation of amorphous metals by mechanical alloying." Materials Science and Engineering **97**(0): 15-23.

22. Schroeder, V., et al. (1998). "Comparison of the corrosion behavior of a bulk amorphous metal, Zr41. 2Ti13. 8Cu12. 5Ni10Be22. 5, with its crystallized form." Scripta Materialia **38**(10): 1481-1486.

23. Miracle, Daniel B. "A structural model for metallic glasses." *Nature materials*3.10 (2004): 697-702.

24. M. Naka, K. Hashimoto, and T. Masumoto: Corrosion resistivity of amorphous iron alloys containing chromium. J. Jpn. Inst. Met. 38, 835 (1974).

25. M. Naka, K. Hashimoto, and T. Masumoto: Corrosion behavior of amorphous and crystalline Cu50Ti50 and Cu50Zr50 alloys. J. Non-Cryst. Solids 30, 29 (1978).

26. Branagan, M. B. "High-Performance Corrosion-Resistant Iron-Based Amorphous Metals-The Effects of Composition, Structure and Environment: Fe49. 7Cr17. 7Mn1. 9Mo7. 4W1. 6B15. 2C3. 8Si2. 4." (2006).

27. Merello, R., et al. "Influence of chemical composition on the pitting corrosion resistance of non-standard low-Ni high-Mn–N duplex stainless steels."*Corrosion Science* 45.5 (2003): 909-921.

28. A. Gebert, J. Eckert, and L. Schultz, Effect of oxygen on phase formation and thermal stability of slowly cooled Zr65Al7.5Cu17.5Ni10 metallic glass, Acta Mater. 46(15), 5475–5482 (1998).

29. C. T. Liu, M. F. Chisholm, and M. K. Miller, Oxygen impurity and microalloying effect in a Zr-based bulk metallic glass alloy, Intermetallics 10(11–12), 1105–1112 (2002).

30. B. S. Murty, D. H. Ping, K. Hono, and A. Inoue, Direct evidence for oxygen stabilization of icosahedral phase during crystallization of Zr65Cu27.5Al7.5 metallic glass, Appl. Phys. Lett. 76(1), 55–57 (2000).

31. D. J. Sordelet, X. Yang, E. A. Rozhkova, M. F. Besser, and M. J. Dramer, Influence of oxygen content in phase selection during quenching of Zr80Pt20 melt spun ribbons, Intermetallics 12(10–11), 1211–1217 (2004).

32. C. T. Liu and Z. P. Lu, Effect of minor alloying additions on glass formation in bulk metallic glasses, Intermetallics 13, 415–418 (2005).

33. A. Inoue, Stabilization of metallic supercooled liquid and bulk amorphous alloys, Acta Mater. 48(1), 279–306 (2000)

34. Wang, A. P., et al. "Corrosion behavior of Ni-based amorphous alloys and their crystalline counterparts." *Corrosion science* 49.6 (2007): 2628-2635.

35. Asami, K., et al. "Effect of Molybdenum on the Anodic Behavior of Amorphous Fe-Cr-Mo-B Alloys in Hydrochloric Acid." *Journal of The Electrochemical Society* 127.10 (1980): 2130-2138.

36. Sorensen, N. R., F. J. Hunkeler, and R. M. Latanision. "The anodic polarization behavior of Fe-Ni-PB and Fe-Ni-Cr-PB amorphous alloys." *Corrosion* 40.11 (1984): 619-624

37.Gu, Xuenan, et al. "Corrosion of, and cellular responses to Mg–Zn–Ca bulk metallic glasses." *Biomaterials* 31.6 (2010): 1093-1103.

38. Brandice A. Green, Peter K. Liaw, and Raymond A. Buchanan† "Chapter 8: Corrosion Behavior", *Bulk Metallic Glasses*, pages: 205-235

39. Naka, M., et al. (1979). "Corrosion-resistant amorphous Fe□C alloys containing chromium and/or molybdenum." Journal of Non-Crystalline Solids **31**(3): 347-354.

40. Lee, H-J., et al. "The corrosion behavior of amorphous and crystalline Ni-10Ta-20P alloys in 12 M HCl." *Corrosion science* 38.8 (1996): 1269-1279.

41. Masumoto, Tsuyoshi, and Koji Hashimoto. "Chemical properties of amorphous metals." *Annual Review of Materials Science* 8.1 (1978): 215-233. [19] Dugdale, J. S., D. Pavuna, and P. Rhodes. "Metallic glasses: properties and applications." *Endeavour* 9.2 (1985): 62-66.

42. Sorensen, N. R., R. B. Diegle, and S. T. Picraux. "Corrosion Behavior of Phosphorus-Implanted Fe-6Cr and Fe-18Cr Amorphous Alloys." *Corrosion* 43.1 (1987): 2-7.

43. Hashimoto, K., et al. "Characteristics of passivity of extremely corrosion-resistant amorphous iron alloys." *Corrosion Science* 16.2 (1976): 71-76.

44. Hashimoto, K., et al. "Characteristics of passivity of extremely corrosion-resistant amorphous iron alloys." *Corrosion Science* 16.2 (1976): 71-76.

45. U. K. Mudali, S. Baunack, J. Eckert, L. Schultz, and A. Gebert, Pitting corrosion of bulk glass-forming zirconium-based alloys, J. Alloys Compd. 377, 290–297 (2004).

46. K. Edalati, N. Rastkhah, A. Kermani, M. Seiedi, A. Movafeghi, The use of radiography for thickness measurement and corrosion monitoring in pipes, International Journal of Pressure Vessels and Piping, Volume 83, Issue 10, October 2006, Pages 736-741, ISSN 0308-0161

47. P. Willems, B. Vaessen, W. Hueck, U. Ewert “Application of CR for corrosion and wall thickness measurements” Insight, 41 (10) (1999), pp. 635–637

48. N. Marstboom “Computed radiography for corrosion and wall thickness measurements” Insight, 41 (5) (1999), pp. 308–309

49. VAIDYA, PR, et al. "Radiographic Evaluation of Corrosion and Deposits in Pipelines: Results of an IAEA Co-ordinated Research Programme."

50. Davis, Joseph R., ed. *Corrosion: Understanding the basics*. ASM International, 2000.

51. Moller, H., E. T. Boshoff, and H. Froneman. "The corrosion behaviour of a low carbon steel in natural and synthetic seawaters." JOURNAL-SOUTH AFRICAN INSTITUTE OF MINING AND METALLURGY 106.8 (2006): 585.

52. S.C. Dexter, Corrosion in Seawater, *Corrosion: Environments and Industries*, Vol 13C, *ASM Handbook*, ASM International, 2006, p 27–41

53. Winston, R. "Uhlig's corrosion handbook." (2000).

54. Robert Baboian “Corrosion Tests and Standards: Application and Interpretation”

55. Robert M. Kain, Walter T. Young “Corrosion Testing in Natural Waters”: Second Volume, Issue 1300

Appendix-I: Significant digits in Corrosion Rate measurement

$$\text{Corrosion Rate} = \frac{(K\ X\ W)}{(A\ X\ T\ X\ D)}\ \text{mm/y}$$

Variable	Represent	Significant digits
K	a constant (depends on corrosion rate unit desired)	3
T	time of exposure in hours	2 or more
A	area in cm2	3
W	mass loss in grams	4
D	density in g/cm3	3

Number of significant digits in corrosion rate should be 3

Appendix II: Inter-Cellular Bonding and Adhesive Failure of AMH

Inter-cellular bonding is critical in honeycombs due to its influence on mechanical strength and weight of the honeycomb. Adhesive bonding and welding have been used in manufacturing of honeycombs. Majority of commercially available metallic honeycombs made using base materials such as Aluminum, Stainless steel and Titanium. All these are either adhesively bonded or welded. Crystalline base materials used are initially tested for weld ability and compatibility with the adhesive before they are used in manufacturing processes. Adhesive bonding, laser spot welding, and resistance spot welding techniques were tested on AMR for use in inter-cellular joining of AMH [ref]. Laser and resistance spot welding resulted in embrittlement of amorphous substrate, increasing the brittleness and decreasing bond strength. Because of embrittlement, adhesives proved to be more effective for inter-cellular joining of AMH [4].

Adhesives selected based on bond strength criteria were tested for strength retention after immersing in 3.5% NaCl solution. A single row of AMH as shown in FIGURE made of 4 different adhesives has been tested for resistance to immersion. All the four failed within 24 hrs of exposure. Lap-joint shear strength test for different exposure times has been done for AF3109 (which has given highest specific strength). Residual force in the teardrop cell is helping in premature failure of the adhesive. Strength of the adhesive reduced to half even in stress-free condition.

Table 8 Time of failure of different adhesives used

Adhesive	**AF3109**	**AF 163U**	**DP110**	**DP8405NS**
Time to failure	<1 hr	<1 hr	<24 hrs.	<24 hrs.

Appendix III: Replicate Cleaning Procedure

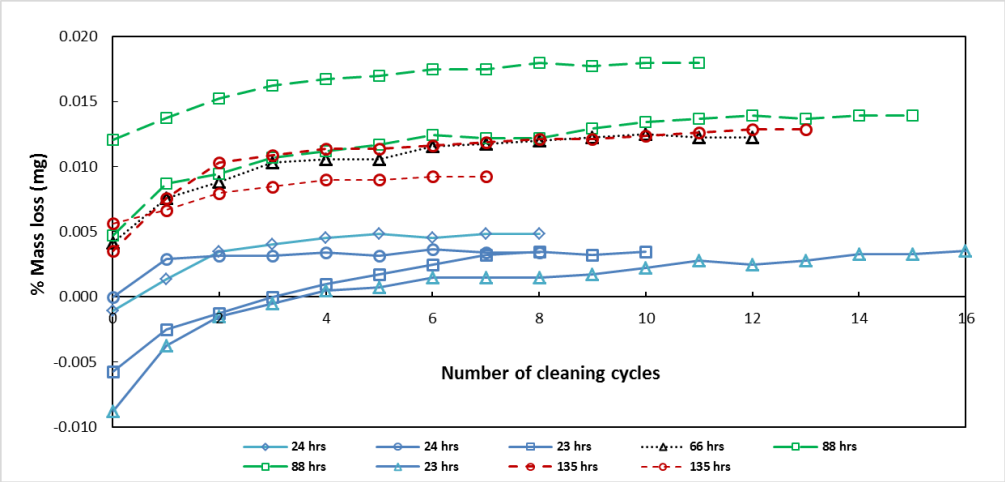

Figure 38 Sample Replicate Cleaning Cycles.

ASTM G1-03 "Standard Practice for Preparing, Cleaning, and Evaluating Corrosion Test Specimens" was followed for cleaning the corroded samples. In this procedure, cleaning cycles are continued until a constant mass loss is observed as shown in Figure 38. Same procedure was followed for all the samples tested during 3.5% NaCl immersion.

VITA

Chandra Sekhar Meduri

Candidate for the Degree of

Master of Science

Thesis: CORROSION RESISTANCE AND MECHANICAL PROPERTIES OF AMORPHOUS METAL HONEYCOMBS

Major Field: Mechanical Engineering

Biographical:

Education:

Completed the requirements for the Master of Science in Mechanical Engineering at Oklahoma State University, Stillwater, Oklahoma in December, 2014.

Completed the requirements for the Bachelor of Technology in Mechanical Engineering at JNTUH College of Engineering, Hyderabad, India in 2012.